



1 **Historical and future contributions of inland waters to the Congo basin**
2 **carbon balance**

3 Adam Hastie^{1,2}, Ronny Lauerwald^{2,3}, Philippe Ciais³, Fabrice Papa^{4,5}, Pierre Regnier²

4

5 ¹School of GeoSciences, University of Edinburgh, EH9 3FF, Edinburgh, Scotland, UK

6 ²Biogeochemistry and Earth System Modelling, Department of Geoscience, Environment and
7 Society, Université Libre de Bruxelles, Bruxelles, 1050, Belgium

8 ³Laboratoire des Sciences du Climat et de l'Environnement (LSCE), CEA CNRS UVSQ, Gif-
9 sur-Yvette 91191, France

10 ⁴Laboratoire d'Etudes en Géophysique et Océanographie Spatiales, Centre National de la
11 Recherche Scientifique–Institut de recherche pour le développement–Université Toulouse Paul
12 Sabatier–Centre national d'études spatiales, 31400 Toulouse, France

13 ⁵Indo-French Cell for Water Sciences, International Joint Laboratory Institut de Recherche
14 pour le Développement and Indian Institute of Science, Indian Institute of Science, 560012
15 Bangalore, India

16

17 *Correspondence to:* Adam Hastie (adam.hastie@ed.ac.uk)

18

19 **Abstract**

20 As the second largest area of contiguous tropical rainforest and second largest river basin in
21 the world, the Congo basin has a significant role to play in the global carbon (C) cycle.

22 Inventories suggest that terrestrial net primary productivity (NPP) and C storage in tree biomass
23 has increased in recent decades in intact forests of tropical Africa, due in large part to a

24 combination of increasing atmospheric CO₂ concentrations and climate change, while

25 rotational agriculture and logging have caused C losses. For the present day, it has been shown

26 that a significant proportion of global terrestrial NPP is transferred laterally to the land-ocean

27 aquatic continuum (LOAC) as dissolved CO₂, dissolved organic carbon (DOC) and particulate

28 organic carbon (POC). Whilst the importance of LOAC fluxes in the Congo basin has been

29 demonstrated for the present day, it is not known to what extent these fluxes have been

30 perturbed historically, how they are likely to change under future climate change and land use



31 scenarios, and in turn what impact these changes might have on the overall C cycle of the basin.
32 Here we apply the ORCHILEAK model to the Congo basin and show that 4% of terrestrial
33 NPP ($NPP = 5,800 \pm 166 \text{ Tg C yr}^{-1}$) is currently exported from soils to inland waters. Further,
34 we found that aquatic C fluxes have undergone considerable perturbation since 1861 to the
35 present day, with aquatic CO_2 evasion and C export to the coast increasing by 26% (186 ± 41
36 Tg C yr^{-1} to $235 \pm 54 \text{ Tg C yr}^{-1}$) and 25% ($12 \pm 3 \text{ Tg C yr}^{-1}$ to $15 \pm 4 \text{ Tg C yr}^{-1}$) respectively,
37 largely because of rising atmospheric CO_2 concentrations. Moreover, under climate scenario
38 RCP 6.0 we predict that this perturbation will continue; over the full simulation period (1861-
39 2099), we estimate that aquatic CO_2 evasion and C export to the coast will increase by 79%
40 and 67% respectively. Finally, we show that the proportion of terrestrial NPP lost to the LOAC
41 also increases from approximately 3% to 5% from 1861-2099 as a result of increasing
42 atmospheric CO_2 concentrations and climate change.

43 **1. Introduction**

44 As the world's second largest area of contiguous tropical rainforest and second largest river,
45 the Congo basin has a significant role to play in the global carbon (C) cycle. Approximately 50
46 Pg C is stored in its above ground biomass (Verhegghen et al., 2012), and up to 100 Pg C
47 contained within its soils (Williams et al., 2007). Moreover, a recent study estimated that
48 around 30 Pg C is stored in the peats of the Congo alone (Dargie et al., 2017). Field data suggest
49 that storage in tree biomass increased by $0.34 \text{ Pg C yr}^{-1}$ in intact African tropical forests
50 between 1968-2007 (Lewis et al., 2009) due in large part to a combination of increasing
51 atmospheric CO_2 concentrations and climate change (Ciais et al., 2009; Pan et al., 2015), while
52 satellite data indicates that terrestrial net primary productivity (NPP) has increased by an
53 average of $10 \text{ g C m}^{-2} \text{ yr}^{-1}$ per year between 2001 and 2013 in tropical Africa (Yin et al., 2017).
54 At the same time, forest degradation, clearing for rotational agriculture and logging are causing
55 C losses to the atmosphere (Zhuravleva et al., 2013; Tyukavina et al., 2018) while droughts



56 have reduced vegetation greenness and water storage over the last decade (Zhou et al., 2014).
57 A recent estimate of above ground C stocks of tropical African forests, mainly in the Congo,
58 indicates a minor net C loss from 2010 to 2017 (Fan et al., 2019).

59 There are large uncertainties associated with projecting future trends in the Congo basin
60 terrestrial C cycle, firstly related to predicting which trajectories of future CO₂ levels and land
61 use changes will occur, and secondly our ability to fully understand and simulate these changes
62 and in turn their impacts. Future model projections for the 21st century agree that temperature
63 will significantly increase under both low and high emission scenarios (Haensler et al., 2013),
64 while precipitation is only projected to substantially increase under high emission scenarios,
65 the basin mean remaining more or less unchanged under low emission scenarios (Haensler et
66 al., 2013). Uncertainties in future land-use change projections for Africa are among the highest
67 for any continent (Hurtt et al., 2011).

68 For the present day at global scale, it has been estimated that between 1 and 5 Pg C yr⁻¹ is
69 transferred laterally to the land-ocean aquatic continuum (LOAC) as dissolved CO₂, dissolved
70 organic carbon (DOC) and particulate organic carbon (POC) (Cole et al., 2007; Battin et al.,
71 2009; Regnier et al., 2013; Drake et al., 2018; Ciais et al. in review). This C can subsequently
72 be evaded back to the atmosphere as CO₂, undergo sedimentation in wetlands and inland
73 waters, or be transported to estuaries or the coast. The tropical region is a hotspot area for
74 inland water C cycling (Lauerwald et al., 2015) due to high terrestrial NPP and precipitation,
75 and a recent study used an upscaling approach based on observations to estimate present day
76 CO₂ evasion from the rivers of the Congo basin at 251±46 Tg C yr⁻¹ and the lateral C (TOC
77 +DIC) export to the coast at 15.5 (13-18) Tg C yr⁻¹ (Borges et al., 2015^a; Borges et al., 2019).
78 To put this into context, their estimate of aquatic CO₂ evasion represents 39% of the global
79 value estimated by Lauerwald et al. (2015, 650 Tg C yr⁻¹) or 14% of the global estimate of
80 Raymond et al. (2013, 1,800 Tg C yr⁻¹).



81 Whilst the importance of LOAC fluxes in the Congo basin has been demonstrated for the
82 present day, it is not known to what extent these fluxes have been perturbed historically, how
83 they are likely to change under future climate change and land use scenarios, and in turn what
84 impact these changes might have on the overall C balance of the Congo. In light of these
85 knowledge gaps, we address the following research questions:

- 86 • What is the relative contribution of LOAC fluxes (CO₂ evasion and C export to the
87 coast) to the present-day C balance of the basin?
- 88 • To what extent have LOAC fluxes changed from 1860 to the present day and what are
89 the primary drivers of this change?
- 90 • How will these fluxes change under future climate and land use change scenarios (RCP
91 6.0 which represents the “no mitigation scenario”) and what are the implications of this
92 change?

93

94 Understanding and quantifying these long-term changes requires a complex and integrated
95 mass-conservation modelling approach. The ORCHILEAK model (Lauerwald et al., 2017), a
96 new version of the land surface model ORCHIDEE (Krinner et al., 2005), is capable of
97 simulating both terrestrial and aquatic C fluxes in a consistent manner for the present day in
98 the Amazon (Lauerwald et al., 2017) and Lena (Bowring et al., 2019^a; Bowring et al., 2019^b)
99 basins. Moreover, it was recently demonstrated that this model could recreate observed
100 seasonal and interannual variation in Amazon aquatic and terrestrial C fluxes (Hastie et al.,
101 2019).

102 In order to accurately simulate aquatic C fluxes, it is crucial to provide a realistic representation
103 of the hydrological dynamics of the Congo River, including its wetlands. Here, we develop
104 new wetland forcing files for the ORCHILEAK model from the high-resolution dataset of
105 Gumbricht et al. (2017) and apply the model to the Congo basin. After validating the model



106 against observations of discharge, flooded area and DOC concentrations for the present day,
107 we then use the model to understand and quantify the long- term (1861-2099) temporal trends
108 in both the terrestrial and aquatic C fluxes of the Congo Basin.

109 **2. Methods**

110 ORCHILEAK (Lauerwald et al., 2017) is a branch of the ORCHIDEE land surface model
111 (LSM), building on past model developments such as ORCHIDEE-SOM (Camino Serrano,
112 2015), and represents one of the first LSM-based approaches which fully integrates the aquatic
113 C cycle within the terrestrial domain. ORCHILEAK simulates DOC production in the canopy
114 and soils, the leaching of dissolved CO₂ and DOC to the river from the soil, the mineralization
115 of DOC, and in turn the evasion of CO₂ to the atmosphere from the water surface. Moreover,
116 it represents the transfer of C between litter, soils and water within floodplains and swamps
117 (see section 2.2). Once within the river routing scheme, ORCHILEAK assumes that the lateral
118 transfer of CO₂ and DOC are proportional to the volume of water. DOC is divided into a
119 refractory and labile pool within the river, with half-lives of 80 and 2 days respectively. The
120 refractory pool corresponds to the combined slow and passive DOC pools of the soil C scheme,
121 and the labile pool corresponds to the active soil pool (see section 2.4.1). The concentration of
122 dissolved CO₂ and the temperature-dependent solubility of CO₂ are used to calculate the partial
123 pressure of CO₂ ($p\text{CO}_2$) in the water column. In turn, CO₂ evasion is calculated based on $p\text{CO}_2$,
124 along with a diurnally variable water surface area and a gas exchange velocity. Fixed gas
125 exchange velocities of 3.5 m d⁻¹ and 0.65 m d⁻¹ respectively are used for rivers (including open
126 floodplains) and forested floodplains.

127 In this study, as in previous studies (Lauerwald et al., 2017, Hastie et al. 2019, Bowring et al.,
128 2019), we run the model at a spatial resolution of 1° and use the default time step of 30 min for
129 all vertical transfers of water, energy and C between vegetation, soil and the atmosphere, and
130 the daily time-step for the lateral routing of water. Until now, in the Tropics, ORCHILEAK



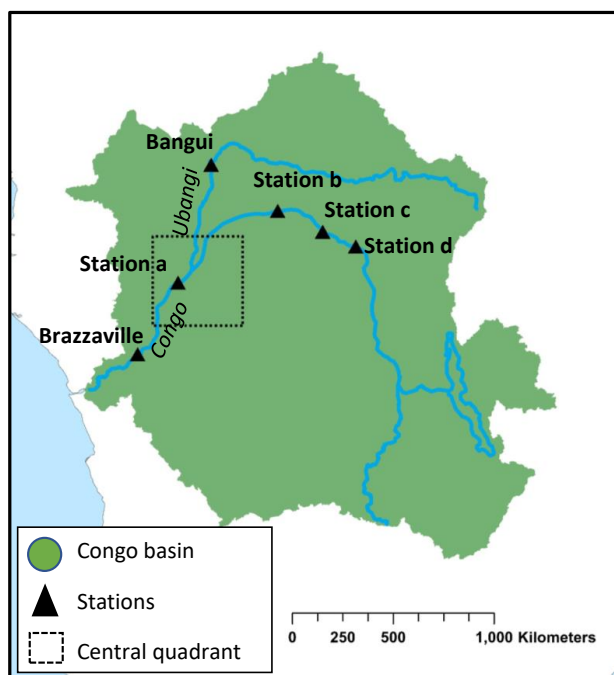
131 has been parameterized and calibrated only for the Amazon River basin (Lauerwald et al., 2017,
132 Hastie et al. 2019). To adapt and apply ORCHILEAK to the specific characteristics of the
133 Congo River basin (2.1), we had to establish new forcing files representing the maximal
134 fraction of floodplains (MFF) and the maximal fraction of swamps (MFS) (2.2) and to
135 recalibrate the river routing module of ORCHILEAK (2.3). All of the processes represented in
136 ORCHILEAK remain identical to those previously represented for the Amazon ORCHILEAK
137 (Lauerwald et al., 2017; Hastie et al., 2019). In the following methodology sections, we
138 describe; 2.1- Congo basin description, 2.2- Development of floodplains and swamps forcing
139 files, 2.3- Calibration of hydrology, 2.4- Simulation set-up, 2.5- Evaluation and analysis of
140 simulated fluvial C fluxes, and 2.6- Calculating the net carbon balance of the Congo Basin. For
141 a full description of the ORCHILEAK model please see Lauerwald et al. (2017).

142 **2.1 Congo basin description**

143 The Congo Basin is the world's second largest area of contiguous tropical rainforest and second
144 largest river basin in the world (Fig. 1), covering an area of $3.7 \times 10^6 \text{ km}^2$, with a mean discharge
145 of around $42,000 \text{ m}^3 \text{ s}^{-1}$ (O'Loughlin et al., 2013) and a variation between 24,700–75,500 m^3
146 s^{-1} across months (Coynel et al., 2005).

147

148



149

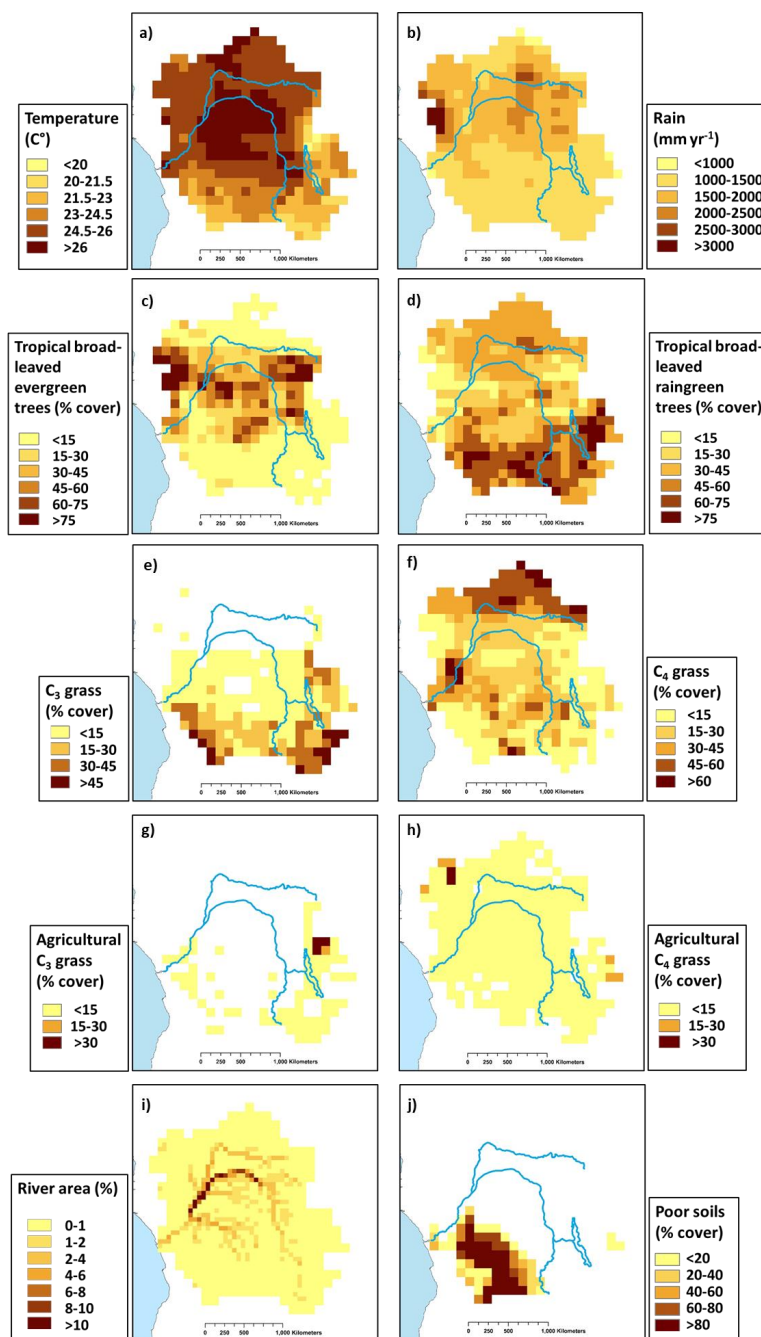
150 **Figure 1: Extent of the Congo Basin, central quadrant of the “Cuvette Centrale” and sampling**
151 **stations (for DOC and discharge) along the Congo and Ubangi Rivers (in italic).**

152

153 The major climate (ISMSIP2b, Frieler et al., 2017; Lang et al., 2017) and land-cover (LUH-
154 CMIP5) characteristics of the Congo Basin for the present day (1981-2010) are shown in Figure
155 2. The mean annual temperature is 25.2 °C but with considerable spatial variation from a low
156 of 18.4°C to a high of 27.2°C (Fig. 2 a), while mean annual rainfall is 1520mm, varying from
157 733 mm to 4087 mm (Fig. 2 b). ORCHILEAK prescribes 13 different plant functional types
158 (PFTs). Land-use is mixed with tropical broad-leaved evergreen (PFT2, Fig. 1 c), tropical
159 broad-leaved rain green (PFT3, Fig. 1 d), C₃ grass (PFT10, Fig. 2 e) and C₄ grass (PFT11, Fig.
160 2 f) covering a maximum of 26%, 35%, 8% and 25% of the basin area respectively (Table A3).
161 Agriculture covers only a small proportion of the basin according to the LUH dataset that is
162 based on FAO cropland area statistics, with C₃ (PFT12, Fig. 2 g) and C₄ (PFT13, Fig. 2 h)
163 agriculture making up a maximum basin area of 0.5 and 2% respectively (Table A3). In reality,
164 a larger fraction of the basin is composed of small scale and rotational agriculture (Tyukavina



165 et al., 2018). The ORCHILEAK model also has a “poor soils” forcing file (Fig. 2 j) which
166 prescribes reduced decomposition rates in soils with low nutrient and pH soils such as Podzols
167 and Arenosols (Lauerwald et al., 2017). This file is developed from the Harmonized World
168 Soil Database (FAO/IIASA/ISRIC/ISS-CAS/JRC, 2009).



169

170 **Figure 2: Present day (1981-2010) spatial distribution of the principal climate and land-use**
 171 **drivers used in ORCHILEAK, across the Congo Basin; a) mean annual temperature in °C, b)**
 172 **mean annual rainfall in mm yr⁻¹, c)-h) mean annual maximum vegetated fraction for PFTs 2,3,**



173 **10,11,12 and 13, i) river area, and j) Poor soils. All at a resolution of 1° except for river area**
174 **(0.5°).**

175 **2.2 Development of floodplains and swamps forcing files**

176 In ORCHILEAK, water in the river network can be diverted to two types of wetlands,
177 floodplains and swamps. In each grid where a floodplain exists, a temporary waterbody can be
178 formed adjacent to the river and is fed by the river once bank-full discharge (see section 2.3)
179 is exceeded. In grids where swamps exist, a constant proportion of river discharge is fed into
180 the base of the soil column. The maximal proportions of each grid which can be covered by
181 floodplains and swamps are prescribed by the maximal fraction of floodplains (MFF) and the
182 maximal fraction of swamps (MFS) forcing files respectively (Guimberteau et al., 2012). See
183 also Lauerwald et al. (2017) and Hastie et al. (2019) for further details. We created an MFF
184 forcing file for the Congo basin, derived from the Global Wetlands^{v3} database; the 232 m
185 resolution tropical wetland map of Gumbricht et al. (2017) (Fig. 3 a and b). We firstly
186 amalgamated all the categories of wetland before aggregating them to a resolution of 0.5° (the
187 resolution at which the floodplain/swamp forcing files are read by ORCHILEAK), assuming
188 that this represents the maximum extent of inundation in the basin. This results in a mean MFF
189 of 10.3%, i.e. a maximum of 10.3% of the surface area of the Congo basin can be inundated
190 with water. This is very similar to the mean MFF value of 10% produced with the Global Lakes
191 and Wetlands Database, GLWD (Lehner, & Döll, P.,2004; Borges et al., 2015^b). We also
192 created an MFS forcing file from the same dataset (Fig. 3 c and d), merging the ‘swamps’ and
193 ‘fens’ wetland categories from Global Wetlands^{v3} database (Gumbricht et al., 2017) and again
194 aggregating them to a 0.5° resolution.

195

196

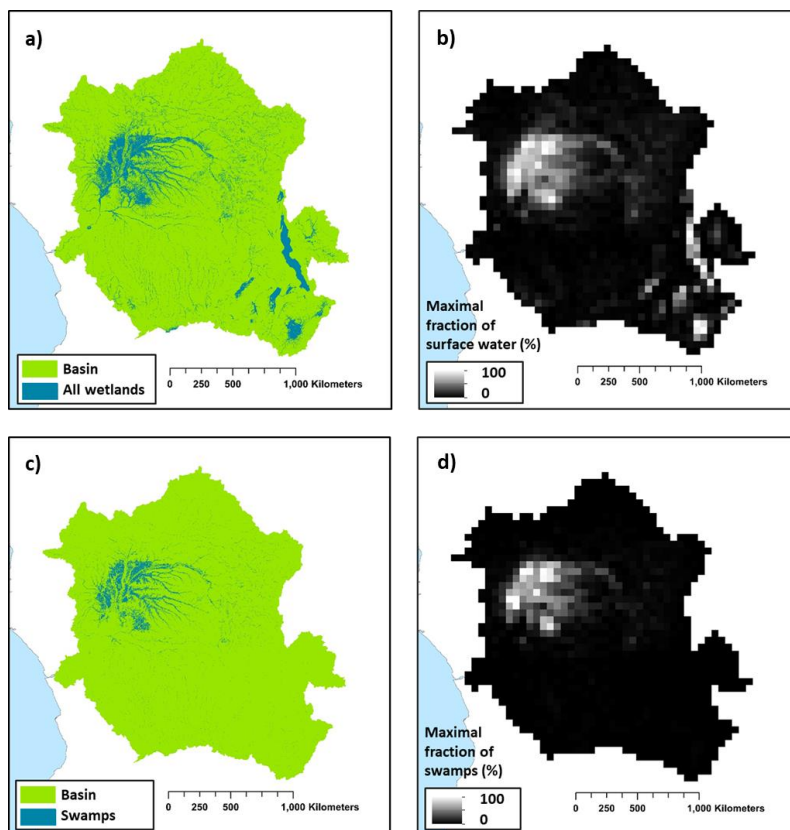


Figure 3: a) Wetland extent (from Gumbricht et al., 2017). b) The new maximal fraction of floodplain (MFF) forcing file developed from a). c) Swamps (including fens) category within Congo basin from Gumbricht et al (2017). d) the new maximal fraction of swamps (MFS) forcing file developed from c). Panels a) and b) are at the same resolution as the Gumbricht dataset (232m) while b) and d) are at a resolution of 0.5°. Note that 0.5° is the resolution of the sub unit basins in ORCHILEAK (Lauerwald et al., 2015), with each 1° grid containing four sub basins.

197

198 2.3 Calibration of hydrology

199 As the main driver of the export of C from the terrestrial to aquatic system, it is crucial that the
200 model can represent present-day hydrological dynamics, at the very least on the main stem of
201 the Congo. As this study is primarily concerned with decadal- centennial timescales our priority
202 was to ensure that the model can accurately recreate observed mean annual discharge at the
203 most downstream gauging station Brazzaville. We also tested the model's ability to simulate



204 observed discharge seasonality, as well as flood dynamics. Moreover, no data is available with
205 which to directly evaluate the simulation of DOC and CO₂ leaching from the soil to the river
206 network, and thus we tested the model's ability to recreate the spatial variation of observed
207 riverine DOC concentrations at specific stations where measurements are available (Borges et
208 al., 2015^b and shown in Fig. 1), river DOC concentration being regarded as an integrator of the
209 C transport at the terrestrial-aquatic interface.

210 We first ran the model for the present-day period, defined as from 1990 to 2005/2010
211 depending on which climate forcing data was applied, using four climate forcing datasets;
212 namely ISIMIP2b (Frieler et al., 2017), Princeton GPCP (Sheffield et al., 2006), GSWP3 (Kim,
213 2017) and CRUNCEP (Viovy, 2018). We used ISIMIP2b for the historical and future
214 simulations as it is the only climate forcing dataset to cover the full period (1861-2099).
215 However, we compared it to other climate forcing datasets for the present day in order to gauge
216 its ability to simulate observed discharge on the Congo River at Brazzaville (Table A1).
217 Without calibration, the majority of the different climate forcing model runs performed poorly,
218 unable to accurately represent the seasonality and mean monthly discharge at Brazzaville
219 (Table A1). The best performing climate forcing dataset was ISIMIP2b followed by Princeton
220 GPCP with root mean square errors (RMSE) of 29% and 40% and Nash Sutcliffe efficiencies
221 (NSE) of 0.20 and -0.25, respectively. NSE is a statistical coefficient specifically used to test
222 the predictive skill of hydrological models (Nash & Sutcliffe, 1970).

223 For ISIMIP2b we further calibrated key hydrological model parameters, namely the constants
224 which dictate the water residence time of the groundwater (=slow reservoir), headwaters (=
225 fast reservoir) and floodplain reservoirs in order to improve the simulation of observed
226 discharge at Brazzaville (Table 2). To do so, we tested different combinations of water
227 residence times for the three reservoirs, eventually settling on 1, 0.5 and 0.5 (days) for the slow,



228 fast and floodplain reservoirs respectively, all three being reduced compared to those values
229 used in the original ORCHILEAK calibration for the Amazon (Lauerwald et al., 2017).

230 In order to calibrate the simulated discharge against observations, we first modified the flood
231 dynamics of ORCHILEAK in the Congo Basin for the present day by adjusting bank-full
232 discharge ($streamr_{50th}$, Lauerwald et al., 2017) and 95th percentile of water level heights
233 ($floodh_{95th}$). As in previous studies on the Amazon basin (Lauerwald et al. 2017, Hastie et al.,
234 2019) we defined bank-full discharge, i.e. the threshold discharge at which floodplain
235 inundation starts, as the median discharge (50th percentile i.e. $streamr_{50th}$) of the present-day
236 climate forcing period (1990 to 2005). After re-running each model parametrization (different
237 water residence times) to obtain those bank-full discharge values, we calculated $floodh_{95th}$ over
238 the simulation period for each grid cell (Table 1). This value is assumed to represent the water
239 level over the river banks at which the maximum horizontal extent of floodplain inundation is
240 reached. We then ran the model for a final time and validated the outputs against discharge
241 data at Brazzaville (Cochonneau et al., 2006, Fig. 1). This procedure was repeated iteratively
242 with the ISIMIP2b climate forcing, modifying the water residence times of each reservoir in
243 order to find the best performing parametrization.

244 Limited observed discharge data is available for the Congo basin, with the majority
245 concentrated on the main stem of the Congo, at Brazzaville station. After comparing simulated
246 vs observed discharge at Brazzaville (NSE, RMSE, Table 2), we used the data of Bouillon et
247 al. (2014) to further validate discharge at Bangui (Fig. 1) on the main tributary Ubangi. In
248 addition, we compared the simulated seasonality of flooded area against the satellite derived
249 dataset GIEMS (Prigent et al., 2007; Becker et al., 2018), within the Cuvette Centrale wetlands
250 (Fig. 1).



251 **2.4 Simulation set-up**

252 A list of the main forcing files used, along with data sources, is presented in Table 1. The
253 derivation of the floodplains and swamp (MFF & MFS) is described in section 2.2 while the
254 calculation of “bankfull discharge” ($\text{streamr}_{50\text{th}}$) and “95th percentile of water table height over
255 flood plain” ($\text{floodh}_{95\text{th}}$) (Table 1) is described in section 2.3.

256 **2.4.1 Soil carbon spin up**

257 ORCHILEAK includes a soil module, primarily derived from ORCHIDEE-SOM (Camino
258 Serrano, 2018). The soil module has 3 different pools of soil DOC; the passive, slow and active
259 pool and these are defined by their source material and residence times (τ_{carbon}). ORCHILEAK
260 also differentiates between flooded and non-flooded soils; decomposition rates of DOC, SOC
261 and litter being reduced (3 times lower) in flooded soils. In order for the soil C pools to reach
262 steady state, we spun-up the model for around 9,000 years, with fixed land-use representative
263 of 1861, and looping over the first 30 years of the ISMSIP2b climate forcing data (1861-1890).
264 During the first 2,000 years of spin-up, we ran the model with an atmospheric CO_2
265 concentration of $350 \mu\text{atm}$ and default soil C residence times (τ_{carbon}) halved, which allowed it
266 to approach steady-state more rapidly. Following this, we ran the model for a further 7,000
267 years reverting to the default τ_{carbon} values. At the end of this process, the soil C pools had
268 reached approximately steady state; $<0.02\%$ change in each pool over the final century of the
269 spin-up.

270 **2.4.2 Transient simulations**

271 After the spin-up, we ran a historical simulation from 1861 until the present day, 2005 in the
272 case of the ISIMIP2b climate forcing data. We then ran a future simulation until 2099, using
273 the final year of the historical simulation as a restart file. In both of these simulations, climate,
274 atmospheric CO_2 and land-cover change were prescribed as fully transient forcings according
275 to the RCP6.0 scenario. For climate variables, we used the IPSL-CM5A-LR model outputs for



276 RCP 6.0, bias corrected by the ISIMIP2b procedure (Frieler et al., 2017; Lange et al., 2017),
277 while land-use change was taken from the 5th Coupled Model Intercomparison Project
278 (CMIP5). As our aim is to investigate long-term trends, we calculated 30-years running means
279 of simulated C flux outputs in order to smooth interannual variations. RCP 6.0 is an emissions
280 pathway that leads to a “stabilization of radiative forcing at 6.0 Watts per square meter (Wm^{-2})
281 in the year 2100 without exceeding that value in prior years” (Masui et al., 2011). It is
282 characterised by intermediate energy intensity, substantial population growth, mid-high C
283 emissions, increasing cropland area to 2100 and decreasing natural grassland area (van Vuuren
284 et al., 2011). In the paper which describes the development of the future land use change
285 scenarios under RCP 6.0 (Hurtt et al., 2011), it is shown that land use change is highly sensitive
286 to land use model assumptions, such as whether or not shifting cultivation is included. In our
287 simulations, shifting cultivation is not included. Moreover, Africa is one the regions with the
288 largest uncertainty range, and thus, there is considerable uncertainty associated with the effect
289 of future land-use change (Hurtt et al., 2011). We chose RCP 6.0 as it represents a no mitigation
290 (mid-high emissions) scenario and because it was the scenario applied in the recent paper of
291 Lauerwald et al. (submitted) to examine the long-term LOAC fluxes in the Amazon basin.
292 Therefore, we can directly compare our results for the Congo to those for the Amazon.
293 Moreover, the ISIMIP2b data only provided two RCPs at the time we performed the
294 simulations; RCP 2.6 (low emission) and RCP 6.0.

295 With the purpose of evaluating separately the effects of land-use change, climate change, and
296 rising atmospheric CO_2 , we ran a series of factorial simulations. In each simulation, one of
297 these factors was fixed at its 1861 level (the first year of the simulation), or in the case of fixed
298 climate change, we looped over the years 1861-1890. The outputs of these simulations (also
299 30-year running means) were then subtracted from the outputs of the main simulation (original



300 run with all factors varied) so that we could determine the contribution of each driver (Fig. 10,
 301 Table 1).

Table 1: Main forcing files used for simulations

Variable	Spatial resolution	Temporal resolution	Data source
Rainfall, snowfall, incoming shortwave and longwave radiation, air temperature, relative humidity and air pressure (close to surface), wind speed (10 m above surface)	1°	1 day	ISIMIP2b, IPSL-CM5A-LR model outputs for RCP6.0 (Frierler et al., 2017)
Land cover (and change)	0.5°	annual	LUH-CMIP5
Poor soils	0.5°	annual	Derived from HWSD v 1.1 (FAO/IIASA/ISRIC/ISS-CAS/JRC, 2009)
Stream flow directions	0.5°	annual	STN-30p (Vörösmarty et al., 2000)
Floodplains and swamps fraction in each grid (MFF & MFS)	0.5°	annual	derived from the wetland high resolution data of Gumbricht et al. (2017)
River surface areas	0.5°	annual	Lauerwald et al. (2015)
Bankfull discharge (streamr _{50th})	1°	annual	derived from calibration with ORCHILEAK (see section 2.3)
95th percentile of water table height over flood plain (floodh _{95th})	1°	annual	derived from calibration with ORCHILEAK (see section 2.3)

302 **2.5 Evaluation and analysis of simulated fluvial C fluxes**

303 We first evaluated DOC concentrations at several locations along the Congo mainstem (Fig.
 304 1), and on the Ubangi river against the data of Borges et al. (2015^b). We also compared the
 305 various simulated components of the net C balance (e.g. NPP) of the Congo against values
 306 described in the literature (Williams et al., 2007; Lewis et al., 2009; Verhegghen et al., 2012;
 307 Valentini et al., 2014; Yin et al., 2017). In addition, we assessed the relationship between the
 308 interannual variation in present day (1981-2010) C fluxes of the Congo basin and variation in
 309 temperature and rainfall. This was done through linear regression using STATISTICA™. We
 310 found trends in several of the fluxes over the 30-year period (1981-2010) and thus detrended
 311 the time series with the “Detrend” function, part of the “SpecsVerification” package in R (R
 312 Core Team 2013), before undertaking the statistical analysis focused on the climate drivers of
 313 inter-annual variability.



314 **2.6 Calculating the net carbon balance of the Congo basin**

315 We calculated Net Ecosystem Production (NEP) by summing the terrestrial and aquatic C
316 fluxes of the Congo basin (Eq. 1), while we incorporated disturbance fluxes (Land-use change
317 flux and harvest flux) to calculate Net Biome Production (NBP) (Eq. 2). Positive values of
318 NBP and NEP equate to a net terrestrial C sink.

319 NEP is defined as follows:

$$320 \quad \quad \quad NEP = NPP + TF - SHR - FCO_2 - LE_{Aquatic} \quad (1)$$

321 Where NPP is terrestrial net primary production, TF is the throughfall flux of DOC from the
322 canopy to the ground, SHR is soil heterotrophic respiration (only that evading from the *terra-*
323 *firme* soil surface); FCO_2 is CO_2 evasion from the water surface and $LE_{Aquatic}$ is the lateral
324 export flux of C (DOC + dissolved CO_2) to the coast. NBP is equal to NEP except with the
325 inclusion of the C lost (or possibly gained) via land use change (LUC) and crop harvest (HAR).
326 Wood harvest is not included for logging and forestry practices, but during deforestation LUC,
327 a fraction of the forest biomass is harvested and channelled to wood product pools with
328 different decay constants. LUC includes land conversion fluxes and the lateral export of wood
329 products biomass, that is, assuming that wood products from deforestation are not consumed
330 and released as CO_2 over the Congo, but in other regions:

$$331 \quad \quad \quad NBP = NEP - (LUC + HAR) \quad (2)$$

332

333 **3. Results**

334 **3.1 Simulation of Hydrology**

335 The final model configuration is able to closely reproduce the mean monthly discharge at
336 Brazzaville (Fig. 4 a), Table 2) and captures the seasonality moderately well (Fig. 4 a, Table 2,

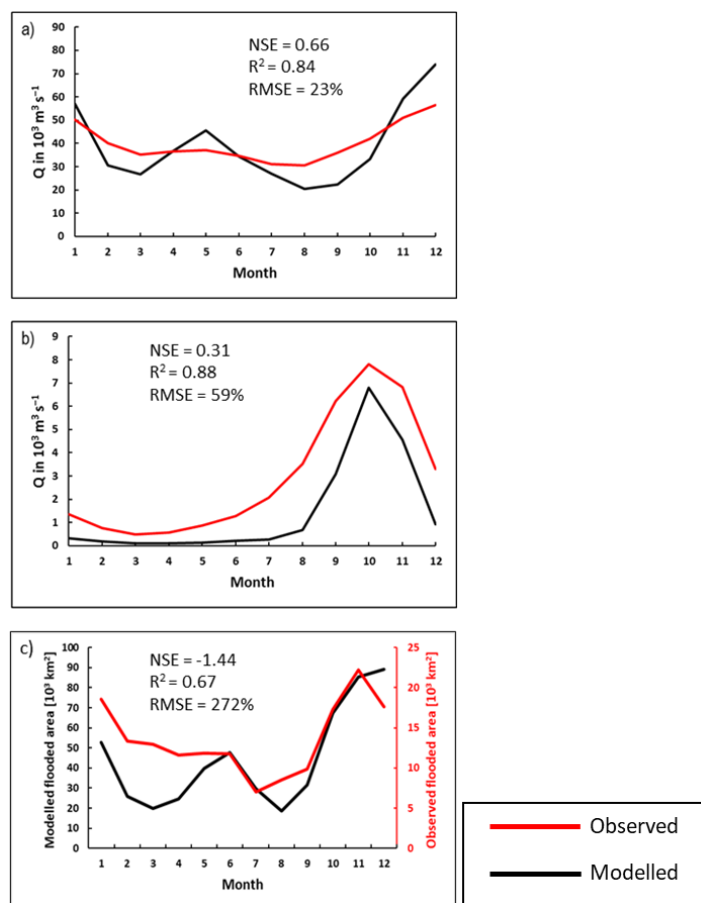


337 RMSE =23%, $R^2 = 0.84$ versus RMSE= 29% and $R^2 = 0.23$ without calibration, Table A1). At
338 Bangui on the Ubangi River (Fig. 1), the model is able to closely recreate observed seasonality
339 (Fig. 4 b), RMSE =59%, $R^2 = 0.88$) but substantially underestimates the mean monthly
340 discharge, our value being only 50% of the observed. We produce reasonable NSE values of
341 0.66 and 0.31 for Brazzaville and Bangui respectively, indicating that the model is moderately
342 accurate in its simulation of seasonality.

343 We also evaluated the simulated seasonal change in flooded area in the central (approx.
344 200,000 km², Fig. 1) part of the Cuvette Centrale wetlands against the GIEMS inundation
345 dataset (1993-2007, maximum inundation minus minimum or permanent water bodies, Prigent
346 et al., 2007; Becker et al., 2018). While our model is able to represent the seasonality in flooded
347 area relatively well ($R^2 = 0.75$ Fig. 4 c), it considerably overestimates the magnitude of flooded
348 area relative to GIEMS (Fig. 4 c, Table 2). However, the dataset that we used to define the
349 MFF and MFS forcing files (Gumbricht et al., 2017) is produced at a higher resolution than
350 GIEMS and will capture smaller wetlands than the GIEMS dataset, and thus the greater flooded
351 area is to be expected. GIEMS is also known to underestimate inundation under vegetated areas
352 (Prigent et al., 2007, Papa et al., 2010) and has difficulties to capture small inundated areas
353 (Prigent et al., 2007; Lauerwald et al., 2017). Indeed, with the GIEMS data we produce an
354 overall flooded area for the Congo Basin of just 3%, less than one-third of that produced with
355 the Gumbricht dataset (Gumbricht et al., 2017) or the GLWD (Lehner, & Döll, P., 2004). As
356 such, it is to be expected that there is a large RMSE (272%, Table 2) between simulated flooded
357 area and GIEMS; more importantly, the seasonality of the two is highly correlated ($R^2 = 0.67$,
358 Table 2). Overall, the hydrological performance of the model against those datasets is
359 satisfactory as the main purpose of this study is to estimate the long-term changes of aquatic C
360 fluxes. In particular, it can closely recreate the mean monthly/annual discharge at Brazzaville



361 (Table 2), the most downstream gauging station on the Congo (Fig. 1). As such, we consider
362 the hydrological performance to be sufficiently good for our aims.



363 **Figure 4: Seasonality of simulated versus observed discharge at a) Brazzaville on the**
364 **Congo (Cochonneau et al., 2006), b) Bangui on the Ubangi (Bouillon et al., 2014) 1990-**
365 **2005 monthly mean and c) flooded area in the the central (approx. 200,000 km²) area of**
366 **the Cuvette Centrale wetlands versus GIEMS (1993-2007, Becker et al., 2018). The**
367 **observed flooded area data represents the maximum minus minimum (permanent water**
368 **bodies such as rivers) GIEMS inundation. See Figure 1 for locations**



Table 2: Performance statistics for modelled versus observed seasonality of discharge and flooded area in Cuvette Centrale

Station	RSME	NSE	R ²	Simulated mean monthly discharge (m ³ s ⁻¹)	Observed mean monthly discharge (m ³ s ⁻¹)
Brazzaville	23%	0.66	0.84	38,944	40,080
Bangui	59%	0.31	0.88	1,448	2,923
				Simulated mean monthly flooded area (10 ³ km ²)	Observed mean monthly flooded area (10 ³ km ²)
Flooded area (Cuvette Centrale)	272%	-1.44	0.67	44	14

369

370 3.2 Carbon fluxes along the Congo basin for the present day

371 For the present day (1981-2010) we estimate a mean annual terrestrial net primary production
 372 (NPP) of 5,800 ±166 (standard deviation, SD) Tg C yr⁻¹ (Fig. 5), corresponding to a mean areal
 373 C fixation rate of approximately 1,500 g C m⁻² yr⁻¹ (Fig. 6 a). We find a significant positive
 374 correlation between the interannual variation of NPP and rainfall (detrended R²= 0.41, p<0.001,
 375 Table A2) and a negative correlation between annual NPP and temperature (detrended R²=
 376 0.32, p<0.01, Table A2). We also see considerable spatial variation in NPP across the Congo
 377 Basin (Fig.6 a).

378 We simulate a mean soil heterotrophic respiration (SHR) of 5,300 ±99 Tg C yr⁻¹ across the
 379 Congo basin (Fig. 5). Contrary to NPP, interannual variation in annual SHR is positively
 380 correlated with temperature (detrended R²= 0.57, p<0.0001, Table A2) and inversely correlated
 381 with rainfall (detrended R²= 0.10), though the latter relationship is not significant (p>0.05).
 382 We estimate a mean annual aquatic CO₂ evasion of rate of 1,363 ±83 g C m⁻² yr⁻¹, amounting



383 to a total of 235 ± 54 Tg C yr⁻¹ across the total water surfaces of the Congo basin (Fig. 5) and
384 attribute 85% of this flux to flooded areas, meaning that only 32 Tg C yr⁻¹ is evaded directly
385 from the river surface. Interannual variation in aquatic CO₂ evasion (1981-2010) shows a
386 strong positive correlation with rainfall (detrended $R^2 = 0.75$, $p < 0.0001$, Table A2) and a weak
387 negative correlation with temperature (detrended $R^2 = 0.09$, not significant, $p > 0.05$). Aquatic
388 CO₂ evasion also exhibits substantial spatial variation (Fig.6, d), displaying a similar pattern to
389 both terrestrial DOC leaching (DOC_{inp}) ($R^2 = 0.81$, $p < 0.0001$, Fig.6, b) as well as terrestrial
390 CO₂ leaching (CO_{2inp}) ($R^2 = 0.96$, $p < 0.0001$, Fig.6, c) into the aquatic system, but not terrestrial
391 NPP ($R^2 = 0.01$, $p < 0.05$, Fig.6, a). We simulate a flux of DOC throughfall from the canopy of
392 27 ± 1 Tg C yr⁻¹.

393 We estimate a mean annual C (DOC + dissolved CO₂) export flux to the coast of 15 ± 4 Tg C
394 yr⁻¹ (Fig. 5). In Figure 7, we compare simulated DOC concentrations at six locations (Fig. 1)
395 along the Congo River and Ubangi tributary, against the observations of Borges et al. (2015^b).
396 We show that we can recreate the spatial variation in DOC concentration within the Congo
397 basin relatively closely with an R^2 of 0.82 and an RMSE of 19% (Fig. 7).

398 For the present day (1981-2010) we estimate a mean annual net ecosystem production (NEP)
399 of 277 ± 137 Tg C yr⁻¹ and a net biome production (NBP) of 107 ± 133 Tg C yr⁻¹ (Fig. 5).
400 Interannually, both NEP and NBP exhibit a strong inverse correlation with temperature
401 (detrended NEP $R^2 = 0.55$, $p < 0.0001$, detrended NBP $R^2 = 0.54$, $p < 0.0001$) and weak positive
402 relationship with rainfall (detrended NEP $R^2 = 0.16$, $p < 0.05$, detrended NBP $R^2 = 0.14$, $p < 0.05$).
403 Furthermore, we simulate a present day (1981-2010) living biomass of 41 ± 1 Pg C and a total
404 soil C stock of 109 ± 1 Pg C.

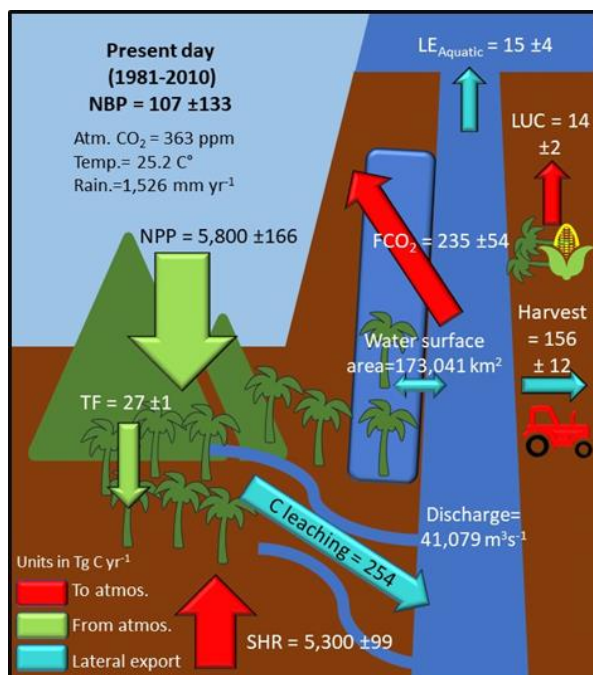
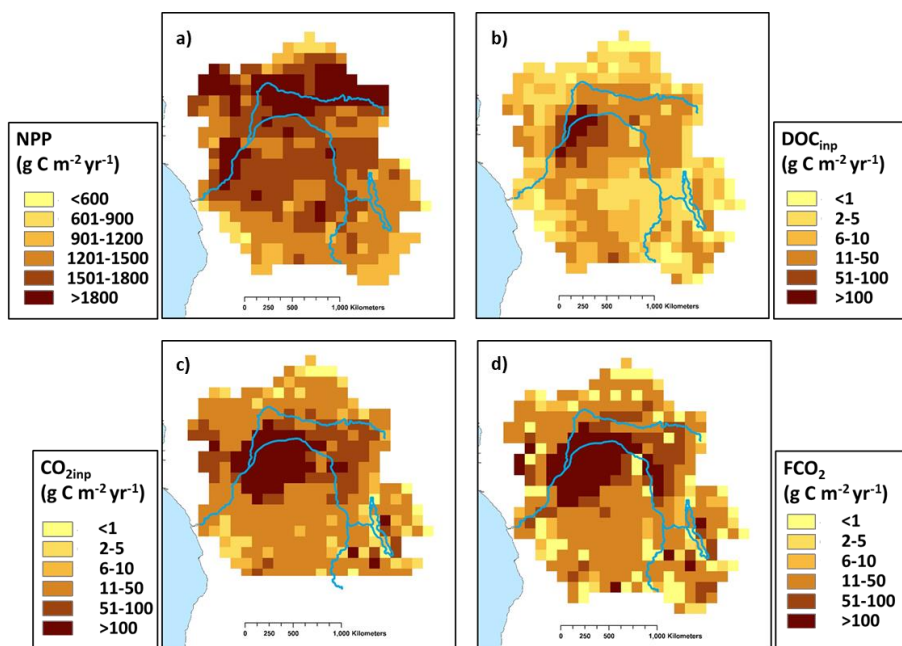


Figure 5: Annual C budget (NBP) for the Congo basin for the present day (1981-2010) simulated with ORCHILEAK, where NPP is terrestrial net primary productivity, TF is throughfall, SHR is soil heterotrophic respiration, FCO₂ is aquatic CO₂ evasion, LOAC is C leakage to the land-ocean aquatic continuum (FCO₂ + LE_{Aquatic}), LUC is flux from Land-use change, and LE_{Aquatic} is the export C flux to the coast. Range represents the standard deviation (SD).

405

406



407

Figure 6: Present day (1981-2010) spatial distribution of a) terrestrial net primary productivity (NPP), b) dissolved organic carbon leaching from soils into the aquatic system (DOC_{inp}), c) CO_2 leaching from soils into the aquatic system ($\text{CO}_{2\text{inp}}$) and d) aquatic CO_2 evasion (FCO_2). Main rivers in blue. All at a resolution of 1°

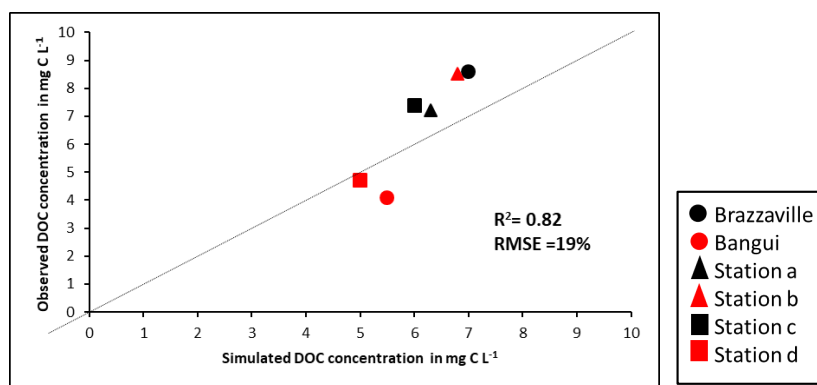


Figure 7: Observed (Borges et al., 2015^a) versus simulated DOC concentrations at several sites along the Congo and Ubangi rivers. See Fig. 1 for locations. The simulated DOC concentrations represent the mean values across the particular sampling period at each site detailed in Borges et al. (2015^a).

408



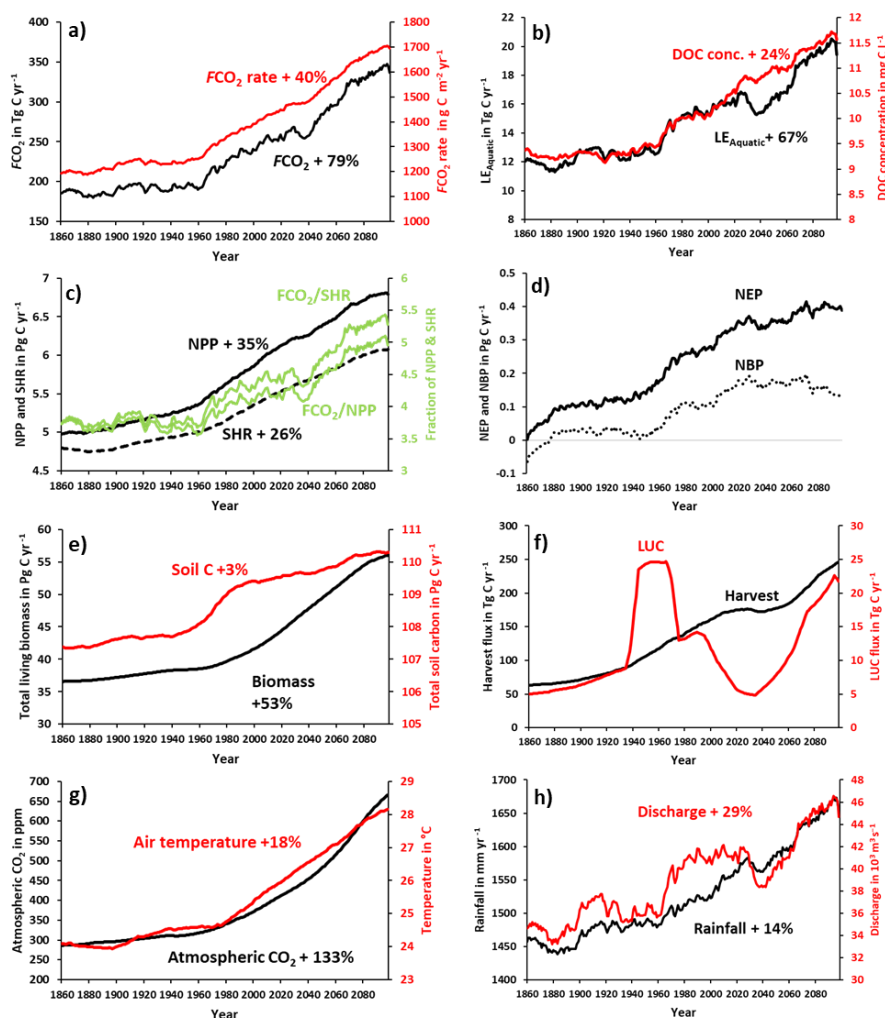
409 **3.3 Long-term temporal trends in carbon fluxes**

410 We find an increasing trend in aquatic CO₂ evasion (Fig. 8 a) throughout the simulation period,
411 rising slowly at first until the 1960s when the rate of increase accelerates. In total CO₂ evasion
412 rose by 79% from 186 Tg C yr⁻¹ at the start of the simulation (1861-1890 mean) (Fig. 9) to 333
413 Tg C yr⁻¹ at the end of this century (2070-2099 mean, Fig. 9), while the increase until the
414 present day (1981-2010 mean) is of +26 % (to 235 Tg C yr⁻¹), though these trends are not
415 uniform across the basin (Fig A1). The lateral export flux of C to the coast (LE_{Aquatic}) follows
416 a similar relative change (Fig. 8b), rising by 67% in total, from 12 Tg C yr⁻¹ (Fig. 9) to 15 Tg
417 C yr⁻¹ for the present day, and finally to 20 Tg C yr⁻¹ (2070-2099 mean, Fig. 9). This is greater
418 than the equivalent increase in DOC concentration (24%, Fig. 8b) due to the concurrent rise in
419 rainfall (by 14%, Fig 8h) and in turn discharge (by 29%, Fig. 8h).

420 Terrestrial NPP and SHR also exhibit substantial increases of 35% and 26% respectively across
421 the simulation period and similarly rise rapidly after 1960 (Fig. 8 c). NEP, NBP (Fig. 8 d) and
422 living biomass (Fig. 8 e) follow roughly the same trend as NPP, but NEP and NBP begin to
423 slow down or even level-off around 2030 and in the case of NBP, we actually simulate a
424 decreasing trend over approximately the final 50 years. Interestingly, the proportion of NPP
425 lost to the LOAC also increases from approximately 3% to 5% (Fig. 8c). We also find that
426 living biomass stock increases by a total of 53% from 1861 to 2099. Total soil C also increases
427 over the simulation but only by 3% from 107 to 110 Pg C yr⁻¹ (Fig. 8 e). Emissions from land-
428 use change (LUC) show considerable decadal fluctuation increasing rapidly in the second half
429 of the 20th century and decreasing in the mid-21st century before rising again towards the end
430 of the simulation (Fig. 8 f). The harvest flux (Fig.8 f) rises throughout the simulation with the
431 exception of a period in the mid-21st century during which it stalls for several decades. This is
432 reflected in the change in land-use areas from 1861- 2099 (Fig. A2, Table A3) during which



433 the natural forest and grassland PFTs marginally decrease while both C₃ and C₄ agricultural
 434 grassland PFTs increase.



435

Figure 8: Simulation results for various C fluxes and stocks from 1861-2099, using IPSL-CM5A-LR model outputs for RCP 6.0 (Frierler et al., 2017). All panels except for atmospheric CO₂, biomass and soil C correspond to 30-year running means of simulation outputs. This was done in order to suppress interannual variation, as we are interested in longer-term trends.

436



437 **3.4 Drivers of simulated trends in carbon fluxes**

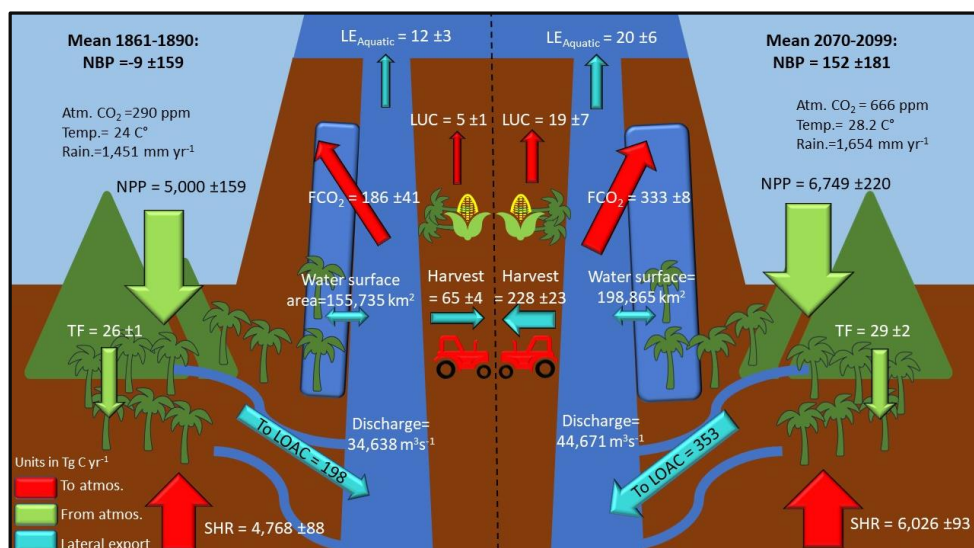
438 The dramatic increase in the concentration of atmospheric CO₂ (Fig. 8 g) and subsequent
439 fertilization effect on terrestrial NPP has the greatest overall impact on all of the fluxes across
440 the simulation period (Fig. 10). It is responsible for the vast majority of the growth in NPP,
441 SHR, aquatic CO₂ evasion and flux of C to the coast (Fig. 10 a, b, c & d). The effect of LUC
442 on these four fluxes is more or less neutral, while the impact of climate change is more varied.
443 The aquatic fluxes (Fig. 10 c, d) respond positively to an acceleration in the increase of both
444 rainfall (and in turn discharge, Fig. 8 h) and temperature (Fig. 8 g) starting around 1970. From
445 around 2020, the impact of climate change on the lateral flux of C to the coast (Fig 10 d) reverts
446 to being effectively neutral, likely a response to a slowdown in the rise of rainfall and indeed a
447 decrease in discharge (Fig 8 h), as well as perhaps the effect of temperature crossing a
448 threshold. The response of the overall loss of terrestrial C to the LOAC (i.e. the ratio of
449 LOAC/NPP, Fig. 10 e) is relatively similar to the response of the individual aquatic fluxes but
450 crucially, climate change exerts a much greater impact, contributing substantially to an increase
451 in the loss of terrestrial NPP to the LOAC in the 1960s, and again in the second half of the 21st
452 century. These changes closely coincide with the pattern of rainfall and in particular with
453 changes in discharge (Fig. 8 h).

454 Overall temperature and rainfall increase by 18% and 14% from 24°C to 28°C and 1457mm to
455 1654mm respectively, but in Fig. A2 one can see that this increase is non-uniform across the
456 basin. Generally speaking, the greatest increase in temperature occurs in the south of the basin
457 while it is the east that sees the largest rise in rainfall (Fig. A2). Land-use changes are similarly
458 non-uniform (Fig. A2).

459 The response of NBP and in NEP (Fig.10 f, g) to anthropogenic drivers is more complex. The
460 simulated decrease in NBP towards the end of the run is influenced by a variety of factors;
461 LUC and climate begin to have a negative effect on NBP (contributing to a decrease in NBP)



462 at a similar time while the positive impact (contributing to an increase in NBP) of atmospheric
 463 CO₂ begins to slow down and eventually level-off (Fig.10 g). LUC continues to have a positive
 464 effect on NEP (Fig.10 f) due to the fact that the expanding C₄ crops have a higher NPP than
 465 forests, while it has an overall negative effect on NBP at the end of the simulation due to the
 466 inclusion of emissions from crop harvest.



467

468 **Figure 9: Annual C budget (NBP) for the Congo basin for; left, the Year 1861 and right, the**
 469 **Year 2099, simulated with ORCHILEAK. NPP is terrestrial net primary productivity, TF is**
 470 **throughfall, SHR is soil heterotrophic respiration, FCO₂ is aquatic CO₂ evasion, LOAC is C**
 471 **leakage to the land-ocean aquatic continuum (FCO₂ + LE_{Aquatic}), LUC is flux from Land-use**
 472 **change, and LE_{Aquatic} is the export C flux to the coast. Range represents the standard deviation**
 473 **(SD).**

474

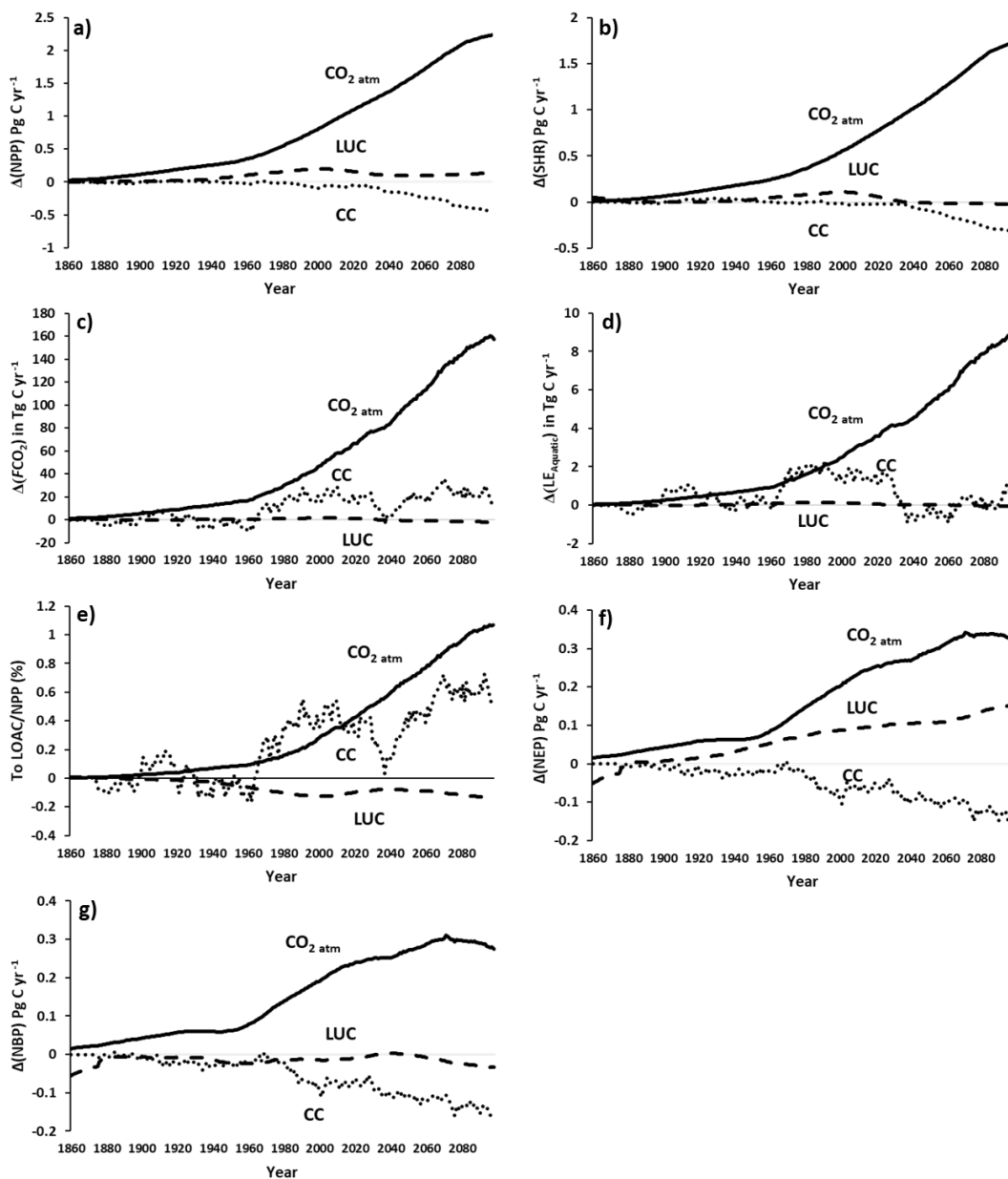
475

476

477



478



479

Figure 10: Contribution of anthropogenic drivers; atmospheric CO₂ concentration (CO_{2 atm}), climate change (CC) and land use change (LUC) to changes in the various carbon fluxes along the Congo Basin, under IPSL-CM5A-LR model outputs for RCP 6.0 (Frierler et al., 2017).

480



481 **4. Discussion**

482 **4.1 Congo basin carbon balance**

483 We simulate a mean present-day terrestrial NPP of approximately $1,500 \text{ g C m}^{-2} \text{ yr}^{-1}$ (Fig. 6),
484 substantially larger than the MODIS derived value of around $1,000 \text{ g C m}^{-2} \text{ yr}^{-1}$ from Yin et al.
485 (2017) across central Africa, though it is important to note that satellite derived estimates of
486 NPP can underestimate the impact of CO_2 fertilization, namely its positive effect on
487 photosynthesis (De Kauwe et al., 2016; Smith et al., 2019). Our stock of the present-day living
488 biomass of 41.1 Pg C is relatively close to the total Congo vegetation biomass of 49.3 Pg C
489 estimated by Verhegghen et al. (2012) based on the analysis of MERIS satellite data. Moreover,
490 our simulated Congo Basin soil C stock of $109 \pm 1.1 \text{ Pg C}$ is consistent with the approximately
491 $120\text{-}130 \text{ Pg C}$ across Africa between the latitudes 10°S to 10°N in the review of Williams et
492 al. (2007), between which the Congo represents roughly 70% of the land area. Therefore, their
493 estimate of soil C stocks across the Congo only would likely be marginally smaller than ours.
494 It is also important to note that neither estimate of soil C stocks explicitly take into account the
495 newly discovered peat store of 30 Pg C (Dargie et al., 2017) and therefore both are likely to
496 represent conservative values. In addition, Williams et al. (2007) estimate the combined fluxes
497 from conversion to agriculture and cultivation to be around 100 Tg C yr^{-1} in tropical Africa
498 (largely synonymous with the Congo Basin), which is relatively close to our present day
499 estimate of harvesting + land-use change flux of 170 Tg C yr^{-1} .

500 Our results suggest that CO_2 evasion from the water surfaces of the Congo is sustained by
501 leaching of dissolved CO_2 and DOC with 226 Tg C and 73 Tg C , respectively, from soils to
502 the aquatic system each year (1980-2010, Fig. 6). Moreover, we find that a disproportionate
503 amount of this transfer occurs (Fig. 6) within the Cuvette Centrale wetland (Fig. 1, Fig. 6) in
504 the centre of the basin, in agreement with a recent study by Borges et al. (2019). In our study,
505 this is due to the large areal proportion of inundated land, facilitating the exchange between



506 soils and aquatic systems. Borges et al. (2019) conducted extensive measurements of DOC
507 and $p\text{CO}_2$, amongst other chemical variables, along the Congo mainstem and its tributaries
508 from Kinshasa in the West of the basin (beside Brazzaville, Fig. 1) through the Cuvette
509 Centrale to Kisangani in the East (close to station d in Fig. 1). They found that both DOC and
510 $p\text{CO}_2$ approximately doubled from Kisangani downstream to Kinshasa, and demonstrated that
511 this variation is overwhelmingly driven by fluvial-wetland connectivity, highlighting the
512 importance of the vast Cuvette Centrale wetland in the aquatic C budget of the Congo basin.

513 Our estimate of the integrated present-day aquatic CO_2 evasion from the river surface of the
514 Congo basin (32 Tg C yr^{-1}) is the same as that estimated by Raymond et al. (2013) (also 32 Tg
515 C yr^{-1}), downscaled over the same basin area, but smaller than the $59.7 \text{ Tg C yr}^{-1}$ calculated by
516 Lauerwald et al. (2015) and far smaller than that of Borges et al. (2015^a), $133\text{-}177 \text{ Tg C yr}^{-1}$ or
517 Borges et al. (2019), $251\pm 46 \text{ Tg C yr}^{-1}$. As previously discussed, we simulate the spatial
518 variation in DOC concentrations measured by Borges et al. (2015^{a,b}, Fig. 7) relatively closely
519 and our mean riverine gas exchange velocity k of 3.5 m d^{-1} is similar to the 2.9 m d^{-1} used by
520 Borges et al. (2015^a). It is therefore somewhat surprising that our estimate of riverine CO_2
521 evasion is so different, and likely to be related to ORCHILEAK underestimating dissolved CO_2
522 inputs into the river network. Below we discuss some possible explanations for this discrepancy
523 related to methodological limitations.

524 One reason for the difference in riverine CO_2 evasion could be that the resolution of
525 ORCHILEAK (1° for C fluxes) is not sufficient to fully capture the dynamics of the smallest
526 streams of the Congo Basin which have been shown to have the highest DOC and CO_2
527 concentrations (Borges et al., 2019). However, it is important to note that in our simulations,
528 the evasion flux from rivers only contributes 15% of total aquatic CO_2 evasion, and including
529 the flux from wetlands/floodplains, we produce a total of 235 Tg C yr^{-1} .



530 Another limitation of the ORCHILEAK model is the lack of representation of aquatic plants.
531 Borges et al. (2019) used the stable isotope composition of $\delta^{13}\text{C-DIC}$ to determine the origin
532 of dissolved CO_2 in the Congo River system and found that the values were consistent with the
533 degradation of organic matter, in particular from C_4 plants. Crucially, they further found that
534 the $\delta^{13}\text{C-DIC}$ values were unrelated to the contribution of *terra-firme* C_4 plants, rather that they
535 were more consistent with the degradation of aquatic C_4 plants, namely macrophytes. This also
536 concurs with the wider conclusions of a previous paper comparing the Congo and the Amazon
537 (Borges et al., 2015^b), which highlighted that aquatic macrophytes are more prevalent in the
538 Congo river and its tributaries compared to the Amazon where strong water currents limit their
539 abundance. The ORCHILEAK model does not represent aquatic plants, and the wider LSM
540 ORCHIDEE does not have an aquatic macrophyte PFT either. This could at least partly explain
541 our conservative estimate of river CO_2 evasion, given that tropical macrophytes have relatively
542 NPP. Rates as high as $3,500 \text{ g C m}^{-2} \text{ yr}^{-1}$ have been measured on floodplains in the Amazon
543 (Silva et al., 2009). While this value is higher than the values represented in the Cuvette
544 Centrale by ORCHILEAK (Figure 6), they are of the same order of magnitude and so this
545 cannot fully explain the discrepancy compared to the results of Borges et al. (2019). In the
546 Amazon basin it has been shown that wetlands export approximately half of their gross primary
547 production (GPP) to the river network compared to upland (*terra-firme*) ecosystems which
548 only export a few percent (Abril et al. 2013). More importantly, Abril et al. (2013) found that
549 tropical aquatic macrophytes exported 80% of their GPP compared to just 36% for flooded
550 forest. Therefore, the lack of a bespoke macrophyte PFT may indeed be one reason for the
551 discrepancy between our results and those of Borges, but largely due to their particularly high
552 export efficiency to the river-floodplain network as opposed to differences in NPP. While being
553 a significant limitation, creating and incorporating a macrophyte PFT would be a substantial
554 undertaking given that the authors are unaware of any published dataset which has



555 systematically mapped their distribution and abundance. It is important to that while
556 ORCHILEAK does not include the export of C from aquatic macrophytes it also neglects their
557 NPP. Moreover, most aquatic macrophytes described in the literature have short (<1 year) life-
558 cycles (Mitchel & Rogers., 1985). As such, this model limitation will only have a very limited
559 net effect on our estimate of the overall annual C balance (NBP, NEP) of the Congo basin, and
560 indeed the other components of NBP.

561 Our simulated export of C to the coast of 15 (15.3) Tg C yr⁻¹ is virtually identical to the
562 TOC+DIC export estimated by Borges et al. (2015^a) of 15.5 Tg C yr⁻¹, which is consistent with
563 the fact that we simulate a similar spatial variation of DOC concentrations (Fig. 7 and Fig. 1
564 for locations). It is also relatively similar to the 19 Tg C yr⁻¹ (DOC + DIC) estimated by
565 Valentini et al. (2014) in their synthesis of the African carbon budget. Valentini et al. (2014)
566 used the largely empirical based Global Nutrient Export from WaterSheds (NEWS) model
567 framework and they point out that Africa was underrepresented in the training data used to
568 develop the regression relationships which underpin the model, and thus this could explain the
569 small disagreement.

570 Our estimate of 4% of NPP per year being transferred to inland waters is substantially lower
571 than that estimated for the Amazon, where around 12% of NPP is lost to the aquatic system
572 each year (Hastie et al., 2019). There are a number of differences between the drivers in the
573 two basins, which could explain this. Mean annual rainfall is 44% greater in the Amazon, and
574 mean annual discharge is 4 times higher, while a maximum of approximately 14% of the
575 surface of the Amazon Basin is covered by water compared to 10% of the Congo (Borges et
576 al., 2015^b; Hastie et al., 2019). Moreover, upland runoff is the main source of water in the
577 wetlands of the Congo as opposed to the Amazon where exchanges between the river and
578 floodplain dominate (Lee et al., 2011; Borges et al., 2015^b). Indeed, the water levels of wetlands
579 in the Congo have been shown to be consistently higher than adjacent river levels (Lee et al.,



580 2011). This also partly explains why for the Congo we find that only 15% of aquatic CO₂
581 evasion comes from the river water surface compared to 25% for the Amazon (Hastie et al.,
582 2019).

583

584 **4.2 Trends in terrestrial and aquatic carbon fluxes**

585 There is sparse observed data available on the long-term trends of terrestrial C fluxes in the
586 Congo. Yin et al. (2017) used MODIS data to estimate NPP between 2001 and 2013 across
587 central Africa. They found that NPP increased on average by 10 g C m⁻² per year, while we
588 simulate an average annual increase of 4 g C m⁻² yr⁻¹ over the same period across the Congo
589 Basin. The two values are not directly comparable as they do not cover precisely the same
590 geographic area but it is encouraging that our simulations exhibit a similar trend to remote
591 sensing data. As previously noted, MODIS derived estimates of NPP do not fully include the
592 effect of CO₂ fertilization (de Kauwe et al., 2016) whereas ORCHILEAK does. Thus, the
593 MODIS NPP product may underestimate the increasing trend in NPP, which would bring our
594 modeled trend further away from this dataset. On the other hand, forest degradation effects and
595 recent droughts have been associated with a decrease of greenness (Zhou et al., 2014) and
596 above ground biomass loss (Qie et al., 2019) in tropical forests.

597 Our results of the historic trend in NEP (not including LUC and harvest fluxes) also generally
598 concur with other modelling studies of tropical Africa (Fisher et al., 2013). Fisher et al. (2013)
599 used nine different land surface models to show that the African tropical biome already
600 represented a natural (i.e. no disturbance, but also neglecting LOAC fluxes) net uptake of
601 around 50 Tg C yr⁻¹ in 1901 and that this uptake more than doubled by 2010. We find a similar
602 trend though we simulate higher absolute NEP. Indeed, one of the models used in Fisher was
603 ORCHIDEE and using this model alone, they calculate a virtually identical estimate of net



604 uptake of 277 Tg C yr⁻¹ for the present day, though this estimate neglects the transfers of C
605 along the LOAC and would therefore be reduced with their inclusion. Our results also generally
606 concur with estimates based on the upscaling of biomass observations (Lewis et al., 2009).
607 Lewis et al. (2009) up-scaled forest plot measurements to calculate that intact tropical African
608 forests represented a net uptake of approximately 300 Tg C yr⁻¹ between 1968 and 2007 and
609 this is consistent with our NEP estimate 275 Tg C yr⁻¹ over the same period.

610 Over the entire simulation period (1861-2099), we estimate that aquatic CO₂ evasion will
611 increase by 79% and the export of C to the coast by 67%. This increase is considerably higher
612 than the 25% and 30% rise in outgassing and export predicted for the Amazon basin (Lauerwald
613 et al., submitted), over the same period and under the same scenario. This is largely due to the
614 fact climate change is predicted to have a substantial negative impact on the aquatic C fluxes
615 in the Amazon, something that we do not find for the Congo where rainfall is projected to
616 substantially increase over the 21st century (RCP 6.0). In the Amazon, Lauerwald et al.
617 (submitted) show that while there are decadal fluctuations in precipitation and discharge, total
618 values across the basin remain unchanged in 2099 compared to 1861. However, changes in the
619 spatial distribution of precipitation mean that the total water surface area actually decreases in
620 the Amazon. Indeed, while we find an increase in the ratio of C exports to the LOAC/NPP from
621 3 to 5%, Lauerwald et al. (submitted) find a comparative decrease. The increase in the
622 proportion of NPP lost to the aquatic system (Fig. 8, 9) as well as in the concentration of DOC
623 (by 24% at Brazzaville) that we find in the Congo, could have important secondary effects, not
624 least the potential for greater DOC concentrations to cause a reduction in pH levels (Laudon &
625 Buffam, 2008) with implications for the wider ecology (Weiss et al., 2018).

626 Our simulated increase in DOC export to the coast up to the present day is smaller than findings
627 recently published for the Mississippi River using the Dynamic Land Ecosystem Model
628 (DLEM, Ren et al., 2016). In addition, the Mississippi study identified LUC including land



629 management practices (e.g. irrigation and fertilization), followed by change in atmospheric
630 CO₂, as the biggest factors in the 40% increase in DOC export to the Gulf of Mexico (Ren et
631 al., 2016). Another recent study (Tian et al., 2015), found an increase in DIC export from
632 eastern North America to the Atlantic Ocean from 1901-2008 but no significant trend in DOC.
633 They demonstrated that climate change and increasing atmospheric CO₂ had a significant
634 positive effect on long-term C export while land-use change had a substantial negative impact.

635 **4.3 Limitations and further model developments**

636 It is important to note that we can have greater confidence in the historic trend (until present-
637 day), as the future changes are reliant on the skill of Earth System model predictions and of
638 course on the accuracy of the RCP 6.0 scenario. There are for example, large uncertainties
639 associated with the future CO₂ fertilization effect (Schimel et al., 2015) and the majority of
640 land surface models, ORCHILEAK included in its current iteration, do not represent the effect
641 of nutrient limitation on plant growth meaning that estimates of land C uptake may be too large
642 (Goll et al., 2017). There are also considerable uncertainties associated with future climate
643 projections in the Congo basin (Haensler et al., 2013). However, in most cases the future trends
644 that we find are more or less continuations of the historic trends, which already represent
645 substantial changes to the magnitude of many fluxes.

646 Moreover, we do not account for methane fluxes from Congo wetlands, estimated at 1.6 to 3.2
647 Tg (CH₄) per year (Tathy et al., 1992), and instead assume that all C is evaded in the form of
648 CO₂. Another limitation is the lack of accounting for bespoke peatland dynamics in the
649 ORCHILEAK model. ORCHILEAK is able to represent the general reduction in C
650 decomposition in water-logged soils and indeed Hastie et al. (2019) demonstrated that
651 increasing the maximum floodplain extent in the Amazon Basin led to an increase in NEP
652 despite fueling aquatic CO₂ evasion because of the effect of reducing soil heterotrophic



653 respiration. Furthermore, ORCHILEAK uses a “poor soils” mask forcing file (Fig. 2 j) based
654 on the Harmonized World Soil Database (FAO/IIASA/ISRIC/ISS-CAS/JRC, 2009), which
655 prescribes reduced decomposition rates in low nutrient and pH soils (e.g. Podzols and
656 Arenosols). The effect of the “poor soils” forcing can clearly be seen in the spatial distribution
657 of the soil C stock in Fig. A3, where the highest C storage coincides with the highest proportion
658 of poor soils. Interestingly, this does not include the Cuvette Centrale wetlands (Fig. 1), an area
659 which was recently identified as containing the world’s largest intact tropical peatland and a
660 stock of around 30 Pg C (Dargie et al., 2017). One potential improvement that could be made
661 to ORCHILEAK would be the development of a new tailored “poor soils” forcing file for the
662 Congo Basin which explicitly includes Histosols, perhaps informed by the Soil Grids database
663 (Hengl et al., 2014), to better represent the Cuvette Centrale. This could in turn, be validated
664 and/or calibrated against the observations of Dargie et al. (2017). A more long-term aim could
665 be the integration/ coupling of the ORCHIDEE-PEAT module with ORCHILEAK.
666 ORCHIDEE- PEAT (Qiu et al., 2019) represents peat as an independent sub-grid hydrological
667 soil unit in which peatland soils are characterized by peat-specific hydrological properties and
668 multi-layered transport of C and water. Thus far, it has only been applied to northern peatlands,
669 and calibrating it to tropical peatlands, along with integrating it within ORCHILEAK would
670 require considerable further model development, but would certainly be a valuable longer-term
671 aspiration. This could also be applied across the tropical region and would allow us to
672 comprehensively explore the implications of climate change and land-use change for tropical
673 peatlands. In addition, ORCHILEAK does not simulate the erosion and subsequent burial of
674 POC within river and floodplain sediments. Although it does not represent the lateral transfer
675 of POC, it does incorporate the decomposition of inundated litter as an important source of
676 DOC and dissolved CO₂ to the aquatic system; i.e. it is assumed that POC from submerged
677 litter decomposes locally in ORCHILEAK. Moreover, previous studies have found that DOC



678 as opposed to POC (Spencer et al., 2016; Bouillon et al., 2012) overwhelmingly dominates the
679 total load of C in the Congo. As previously noted, the representation of the rapid C loop of
680 aquatic macrophytes should also be made a priority in terms of improving models such as
681 ORCHILEAK, particularly in the tropics. For further discussion of the limitations of
682 ORCHILEAK, please also see Lauerwald et al. (2017) and Hastie et al. (2019).

683 **5. Conclusions**

684 For the present day, we show that aquatic C fluxes, and in particular CO₂ evasion, are important
685 components of the Congo Basin C balance, larger than for example the combined fluxes from
686 LUC and harvesting, with around 4% of terrestrial NPP being exported to the aquatic system
687 each year. We find that these fluxes have undergone considerable perturbation since 1861 to
688 the present day, and that under RCP 6.0 this perturbation will continue; over the entire
689 simulation period (1861-2099), we estimate that aquatic CO₂ evasion will increase by 79% and
690 the export of C to the coast by 67%. We further find that the ratio of C exports to the
691 LOAC/NPP increases from 3 to 5%, driven by both rising atmospheric CO₂ concentrations and
692 climate change. The increase in the proportion of NPP transferred to the aquatic system (Fig.
693 8, 9), as well as in the concentration of DOC (by 24% at Brazzaville), could also have important
694 secondary effects, not least the potential for greater DOC concentrations to cause a reduction
695 in pH levels (Laudon & Buffam, 2008) with implications for the wider ecology (Weiss et al.,
696 2018). This calls for long-term monitoring of C levels and fluxes in the rivers of the Congo
697 basin, and further investigation of the potential impacts of such change, including additional
698 model developments.

699

700 *Code availability.* A description of the general ORCHIDEE code can be found here:
701 http://forge.ipsl.jussieu.fr/orchidee/browser#tags/ORCHIDEE_1_9_6/ORCHIDEE.



702 The main part of the ORCHIDEE code was written by Krinner et al. (2005). See d'Orgeval et
703 al. (2008) for a general description of the river routing scheme. For the updated soil C module
704 please see Camino Serrano (2015). For the source code of ORCHILEAK see Lauerwald et al.
705 (2017)- <https://doi.org/10.5194/gmd-10-3821-2017-supplement>

706 For details on how to install ORCHIDEE and its various branches, please see the user guide:
707 <http://forge.ipsl.jussieu.fr/orchidee/wiki/Documentation/UserGuide>

708 *Author contribution.* AH, RL, PR and PC all contributed to the conceptualization of the study.
709 RL developed the model code, AH developed the novel forcing files for Congo, and AH
710 performed the simulations. FP provided the GIEMS dataset for model validation. AH prepared
711 the manuscript with contributions from all co-authors. RL and PR provided supervision and
712 guidance to AH throughout the research. PR acquired the primary financial support that
713 supported this research.

714 *Competing interests.* The authors declare that they have no conflict of interest.

715 *Financial support.* Financial support was received from the European Union's Horizon 2020
716 research and innovation programme under the Marie Skłodowska- Curie grant agreement No.
717 643052 (C-CASCADES project). PR acknowledges funding from the European Union's
718 Horizon 2020 research and innovation programme under Grant Agreement 776810 (project
719 VERIFY). RL acknowledges funding from the ANR ISIPEDIA ERA4CS project.

720

721 **References**

722 Abril, G., Martinez, J.-M., Artigas, L. F., Moreira-Turcq, P., Benedetti, M. F., Vidal, L., ...
723 Roland, F. (2013). Amazon River carbon dioxide outgassing fuelled by wetlands. *Nature*,
724 *505*, 395. Retrieved from <http://dx.doi.org/10.1038/nature12797>

725 Battin, T. J., Luyssaert, S., Kaplan, L. A., Aufdenkampe, A. K., Richter, A., & Tranvik, L. J.
726 (2009). The boundless carbon cycle. *Nature Geoscience*, *2*, 598. Retrieved from
727 <https://doi.org/10.1038/ngeo618>



- 728 Becker, M.; Papa, F.; Frappart, F.; Alsdorf, D.; Calmant, S.; Da Silva, J.S.; Prigent, C.;
729 Seyler, F. Satellite-based estimates of surface water dynamics in the Congo River Basin. *Int.*
730 *J. Appl. Earth Obs. Geoinf.* 2018, 196–209
- 731 Borges, A. V., Darchambeau, F., Teodoru, C. R., Marwick, T. R., Tamooch, F., Geeraert, N.,
732 ... Bouillon, S. (2015)^a. Globally significant greenhouse-gas emissions from African inland
733 waters. *Nature Geoscience*, 8, 637. Retrieved from <https://doi.org/10.1038/ngeo2486>
- 734 Borges, A. V., Abril, G., Darchambeau, F., Teodoru, C. R., Deborde, J., Vidal, L. O., ...
735 Bouillon, S. (2015)^b. Divergent biophysical controls of aquatic CO₂ and CH₄ in the World's
736 two largest rivers. *Scientific Reports*, 5, 15614. <https://doi.org/10.1038/srep15614>
- 737 Borges, A. V., Darchambeau, F., Lambert, T., Morana, C., Allen, G. H., Tambwe, E.,
738 Toengaho Sembaito, A., Mambo, T., Nlandu Wabakhangazi, J., Descy, J.-P., Teodoru, C. R.,
739 and Bouillon, S (2019): Variations in dissolved greenhouse gases (CO₂, CH₄, N₂O) in the
740 Congo River network overwhelmingly driven by fluvial-wetland connectivity,
741 *Biogeosciences*, 16, 3801–3834, <https://doi.org/10.5194/bg-16-3801-2019>.
- 742 Bouillon, S., Yambélé, A., Spencer, R. G. M., Gillikin, D. P., Hernes, P. J., Six, J., Merckx,
743 R., and Borges, A. V.: Organic matter sources, fluxes and greenhouse gas exchange in the
744 Oubangui River (Congo River basin), *Biogeosciences*, 9, 2045–2062,
745 <https://doi.org/10.5194/bg-9-2045-2012>, 2012.
- 746 Bouillon, S., Yambélé, A., Gillikin, D. P., Teodoru, C., Darchambeau, F., Lambert, T., &
747 Borges, A. V. (2014). Contrasting biogeochemical characteristics of the Oubangui River and
748 tributaries (Congo River basin). *Scientific Reports*, 4, 5402. Retrieved from
749 <https://doi.org/10.1038/srep05402>
- 750 Bowring, S. P. K., Lauerwald, R., Guenet, B., Zhu, D., Guimberteau, M., Tootchi, A.,
751 Ducharne, A., and Ciais, P (2019)^a: ORCHIDEE MICT-LEAK (r5459), a global model for
752 the production, transport, and transformation of dissolved organic carbon from Arctic
753 permafrost regions – Part 1: Rationale, model description, and simulation protocol, *Geosci.*
754 *Model Dev.*, 12, 3503–3521, <https://doi.org/10.5194/gmd-12-3503-2019>, 2019.
- 755 Bowring, S. P. K., Lauerwald, R., Guenet, B., Zhu, D., Guimberteau, M., Regnier, P.,
756 Tootchi, A., Ducharne, A., and Ciais, P (2019)^b: ORCHIDEE MICT-LEAK (r5459), a global
757 model for the production, transport and transformation of dissolved organic carbon from
758 Arctic permafrost regions, Part 2: Model evaluation over the Lena River basin, *Geosci.*
759 *Model Dev. Discuss.*, <https://doi.org/10.5194/gmd-2018-322>, in review, 2019.
- 760 Camino-Serrano, M., Guenet, B., Luysaert, S., & Janssens, I. A. (2018). ORCHIDEE-SOM:
761 modeling soil organic carbon (SOC) and dissolved organic carbon (DOC) dynamics along
762 vertical soil profiles in Europe. *Geoscientific Model*
763 *Development* , 11, 937– 957. <https://doi.org/10.5194/gmd-11-937-2018>
- 764 Ciais, P., Piao, S.-L., Cadule, P., Friedlingstein, P., & Chédin, A. (2009). Variability and
765 recent trends in the African terrestrial carbon balance. *Biogeosciences*, 6(9), 1935–1948.
766 <https://doi.org/10.5194/bg-6-1935-2009>



- 767 Ciais, P., Gasser, T., Lauerwald, R., Peng, S., Raymond, P. A., Wang, Y., Zhu, D. (2017).
768 Observed regional carbon budgets imply reduced soil heterotrophic respiration. *Nature*, in
769 review.
- 770 Cochonneau, G., Sondag, F., Guyot, J.-L., Geraldo, B., Filizola, N., Fraizy, P., Laraque, A.,
771 Magat, P., Martinez, J.-M., Noriega, L., Oliveira, E., Ordonez, J., Pombosa, R., Seyler, F.,
772 Sidgwick, J., and Vauchel, P.: The environmental observation and research project, ORE
773 HYBAM, and the rivers of the Amazon basin, in: *Climate Variability and Change –*
774 *Hydrological Impacts*, IAHS Publ. 308, edited by: Demuth, S., Gustard, A., Planos, E.,
775 Scatena, F., and Servat, E., IAHS Press, UK, 44–50, 2006
- 776 Coynel, A., P. Seyler, H. Etcheber, M. Meybeck, and D. Orange (2005), Spatial and seasonal
777 dynamics of total suspended sediment and organic carbon species in the Congo River, *Global*
778 *Biogeochem. Cycles*, 19, GB4019, doi:[10.1029/2004GB002335](https://doi.org/10.1029/2004GB002335).
- 779 Creese, A., Washington, R., & Jones, R. (2019). Climate change in the Congo Basin:
780 processes related to wetting in the December–February dry season. *Climate Dynamics*, 53(5),
781 3583–3602. <https://doi.org/10.1007/s00382-019-04728-x>
- 782 Dargie, G. C., Lewis, S. L., Lawson, I. T., Mitchard, E. T. A., Page, S. E., Bocko, Y. E., &
783 Ifo, S. A. (2017). Age, extent and carbon storage of the central Congo Basin peatland
784 complex. *Nature*, 542, 86. Retrieved from <https://doi.org/10.1038/nature21048>
- 785 De Kauwe, M. G., Keenan, T. F., Medlyn, B. E., Prentice, I. C. and Terrer, C. (2016) Satellite
786 based estimates underestimate the effect of CO₂ fertilisation on net primary
787 productivity. *Nature Climate Change*, 6, 892-893
- 788 d'Orgeval, T., Polcher, J., & de Rosnay, P. (2008). Sensitivity of the West African
789 hydrological cycle in ORCHIDEE to infiltration processes. *Hydrology and Earth System*
790 *Sciences*, 12, 1387–1401. <https://doi.org/10.5194/hess-12-1387-2008>
- 791 Drake, T. W., Raymond, P. A., & Spencer, R. G. M. (2018). Terrestrial carbon inputs to
792 inland waters: A current synthesis of estimates and uncertainty. *Limnology and*
793 *Oceanography Letters*, 3(3), 132–142. <http://doi.org/10.1002/lol2.10055>
- 794 Fan, L., Wigneron, J.-P., Ciais, P., Chave, J., Brandt, M., Fensholt, R., ... Peñuelas, J. (2019).
795 Satellite-observed pantropical carbon dynamics. *Nature Plants*, 5(9), 944–951.
796 <https://doi.org/10.1038/s41477-019-0478-9>
- 797 FAO/IIASA/ISRIC/ISS-CAS/JRC: Harmonized World Soil Database (version 1.1), FAO,
798 Rome, 2009.
- 799 Fisher JB, Sikka M, Sitch S, Ciais P, Poulter B, Galbraith D, Lee J-E, Huntingford C, Viovy
800 N, Zeng N, Ahlstrom A, Lomas MR, Levy PE, Frankenberg C, Saatchi S, Malhi Y. 2013
801 African tropical rainforest net carbon dioxide fluxes in the twentieth century. *Phil Trans R*
802 *Soc B* 368: 20120376. <http://dx.doi.org/10.1098/rstb.2012.0376>
- 803 Frieler, K., Lange, S., Piontek, F., Reyer, C. P. O., Schewe, J., Warszawski, L., ... Yamagata,
804 Y. (2017). Assessing the impacts of 1.5 °C global warming – simulation protocol of the Inter-
805 Sectoral Impact Model Intercomparison Project (ISIMIP2b). *Geosci. Model Dev.*, 10(12),
806 4321–4345. <https://doi.org/10.5194/gmd-10-4321-2017>



- 807 Goll, D. S., Vuichard, N., Maignan, F., Jornet-Puig, A., Sardans, J., Violette, A., Peng, S.,
808 Sun, Y., Kvakic, M., Guimberteau, M., Guenet, B., Zaehle, S., Penuelas, J., Janssens, I., and
809 Ciais, P.: A representation of the phosphorus cycle for ORCHIDEE (revision 4520), *Geosci.*
810 *Model Dev.*, 10, 3745–3770, <https://doi.org/10.5194/gmd-10-3745-2017>, 2017.
- 811 Guimberteau, M., Drapeau, G., Ronchail, J., Sultan, B., Polcher, J., Martinez, J.-M., Prigent,
812 C., Guyot, J.-L., Cochonneau, G., Espinoza, J. C., Filizola, N., Fraizy, P., Lavado, W., De
813 Oliveira, E., Pombosa, R., Noriega, L., and Vauchel, P.: Discharge simulation in the sub-
814 basins of the Amazon using ORCHIDEE forced by new datasets, *Hydrol. Earth Syst. Sci.*, 16,
815 911–935, <https://doi.org/10.5194/hess-16-911-2012>, 2012.
- 816 Gumbrecht, T., Roman-Cuesta, R. M., Verchot, L., Herold, M., Wittmann, F., Householder,
817 E., Murdiyarso, D. (2017). An expert system model for mapping tropical wetlands and
818 peatlands reveals South America as the largest contributor. *Global Change Biology*, 23(9),
819 3581–3599. <https://doi.org/10.1111/gcb.13689>
- 820 Haensler, A., Saeed, F. and Jacob, D. (2013): Assessment of projected climate change signals
821 over central Africa based on a multitude of global and regional climate projections. In:
822 Climate Change Scenarios for the Congo Basin. [Haensler A., Jacob D., Kabat P., Ludwig F.
823 (eds.)]. Climate Service Centre Report No. 11, Hamburg, Germany, ISSN: 2192-4058
- 824 Hastie, A., Lauerwald, R., Ciais, P., Regnier, P (2019). Aquatic carbon fluxes dampen the
825 overall variation of net ecosystem productivity in the Amazon basin: An analysis of the
826 interannual variability in the boundless carbon cycle. *Global Change*
827 *Biology*,; 25: 2094– 2111. <https://doi.org/10.1111/gcb.14620>
- 828 Hengl, T., de Jesus, J. M., MacMillan, R. A., Batjes, N. H., Heuvelink, G. B. M., Ribeiro, E.,
829 ... Ruiperez Gonzalez, M. (2014). SoilGrids1km-global soil information based on automated
830 mapping. *PLoS One*, 9, e105992. <https://doi.org/10.1371/journal.pone.0105992>
- 831 Hurtt, G. C., Chini, L. P., Frohling, S., Betts, R. A., Feddema, J., Fischer, G., ... Wang, Y. P.
832 (2011). Harmonization of land-use scenarios for the period 1500–2100: 600 years of global
833 gridded annual land-use transitions, wood harvest, and resulting secondary lands. *Climatic*
834 *Change*, 109(1), 117. <https://doi.org/10.1007/s10584-011-0153-2>
- 835 Kim, H. (2017). *Global Soil Wetness Project Phase 3 Atmospheric Boundary Conditions*
836 *(Experiment 1)* [Data set]. Data Integration and Analysis System (DIAS).
837 <https://doi.org/10.20783/DIAS.501>
- 838 Lange., S (2017). "ISIMIP2b Bias-Correction Code," *Zenodo*, doi: [10.5281/zenodo.1069050](https://doi.org/10.5281/zenodo.1069050)
- 839 Laudon, H., and I. Buffam (2008), Impact of changing DOC concentrations on the potential
840 distribution of acid sensitive biota in a boreal stream network, *Hydrol. Earth Syst.*
841 *Sci.*, 12(2), 425–435.
- 842 Lauerwald, R., Laruelle, G. G., Hartmann, J., Ciais, P., & Regnier, P. A. G. (2015). Spatial
843 patterns in CO₂ evasion from the global river network. *Global Biogeochemical Cycles*, 29(5),
844 534–554. <https://doi.org/10.1002/2014GB004941>
- 845 Lauerwald, R., Regnier, P., Camino-Serrano, M., Guenet, B., Guimberteau, M., Ducharne,
846 A., ... Ciais, P. (2017). ORCHILEAK (revision 3875): a new model branch to simulate



- 847 carbon transfers along the terrestrial--aquatic continuum of the Amazon basin. *Geoscientific*
848 *Model Development*, 10(10), 3821–3859. <https://doi.org/10.5194/gmd-10-3821-2017>
- 849 Lauerwald, R., Regnier, P., Guenet, B., Friedlingstein, P; Ciais, P: How simulations of the
850 land carbon sink are biased by ignoring fluvial carbon transfers – A case study for the
851 Amazon basin, submitted to *One Earth*.
- 852 Lee, H., Beighley, R. E., Alsdorf, D., Jung, H. C., Shum, C. K., Duan, J., ... Andreadis, K.
853 (2011). Characterization of terrestrial water dynamics in the Congo Basin using GRACE and
854 satellite radar altimetry. *Remote Sensing of Environment*, 115(12), 3530–3538.
855 <https://doi.org/https://doi.org/10.1016/j.rse.2011.08.015>
- 856 Lehner, B., & Döll, P. (2004). Development and validation of a global database of lakes,
857 reservoirs and wetlands. *Journal of Hydrology*, 296(1–4), 1–22.
858 <https://doi.org/https://doi.org/10.1016/j.jhydrol.2004.03.028>
- 859 Lewis, S. L., Lopez-Gonzalez, G., Sonké, B., Affum-Baffoe, K., Baker, T. R., Ojo, L. O., ...
860 Wöll, H. (2009). Increasing carbon storage in intact African tropical forests. *Nature*, 457,
861 1003. Retrieved from <https://doi.org/10.1038/nature07771>
- 862 Masui, T., Matsumoto, K., Hijioka, Y., Kinoshita, T., Nozawa, T., Ishiwatari, S., Kato, E.,
863 Shukla, P.R., Yamagata, Y., Kainuma, M., 2011. A emission pathway to stabilize at 6 W/m²
864 of radiative forcing, *Climatic Change*, doi:10.1007/s10584-011-0150-5. Morgan, M.G.,
865 Adams, P., Keith, D.W., 2006. Elicitation of expert judgments of aerosol forcing. *Climatic*
866 *Change* 75, 195–214
- 867 Mitchell D.S., Rogers K.H. (1985) Seasonality/aseasonality of aquatic macrophytes in
868 Southern Hemisphere inland water. In: Davies B.R., Walmsley R.D. (eds) *Perspectives in*
869 *Southern Hemisphere Limnology. Developments in Hydrobiology*, vol 28. Springer,
870 Dordrecht
- 871 Nash, J. E., and J. V. Sutcliffe. 1970. River flow forecasting through conceptual models: Part
872 1. A discussion of principles. *J. Hydrology* 10(3): 282-290
- 873 O'Loughlin, F., M. A. Trigg, G. J.-P. Schumann, and P. D. Bates (2013), Hydraulic
874 characterization of the middle reach of the Congo River, *Water Resour. Res.*, 49, 5059–5070,
875 doi:[10.1002/wrcr.20398](https://doi.org/10.1002/wrcr.20398).
- 876 Pan, S., Dangal, S. R. S., Tao, B., Yang, J., & Tian, H. (2015). Recent patterns of terrestrial
877 net primary production in Africa influenced by multiple environmental changes. *Ecosystem*
878 *Health and Sustainability*, 1(5), 1–15. <https://doi.org/10.1890/EHS14-0027.1>
- 879 Papa, F., Prigent, C., Aires, F., Jimenez, C., Rossow, W. B., and Matthews,
880 E. (2010), Interannual variability of surface water extent at the global scale, 1993–2004, *J.*
881 *Geophys. Res.*, 115, D12111, doi:[10.1029/2009JD012674](https://doi.org/10.1029/2009JD012674).
- 882 Potter, C., Klooster, S., & Genovese, V. (2012). Net primary production of terrestrial
883 ecosystems from 2000 to 2009. *Climatic Change*, 115(2), 365–378.
884 <https://doi.org/10.1007/s10584-012-0460-2>



- 885 Prigent, C., Papa, F., Aires, F., Rossow, W. B., and Matthews, E.: Global inundation
886 dynamics inferred from multiple satellite observations, 1993–2000, *J. Geophys. Res.*, 112,
887 D12107, <https://doi.org/10.1029/2006jd007847>, 2007.
- 888 Qie, L., Telford, E. M., Massam, M. R., Tangki, H., Nilus, R., Hector, A., & Ewers, R. M.
889 (2019). Drought cuts back regeneration in logged tropical forests. *Environmental Research*
890 *Letters*, 14(4), 45012. <https://doi.org/10.1088/1748-9326/ab0783>
- 891 Qiu, C., Zhu, D., Ciais, P., Guenet, B., Peng, S., Krinner, G., Tootchi, A., Ducharne, A., and
892 Hastie, A.: Modelling northern peatland area and carbon dynamics since the Holocene with
893 the ORCHIDEE-PEAT land surface model (SVN r5488), *Geosci. Model Dev.*, 12, 2961–
894 2982, <https://doi.org/10.5194/gmd-12-2961-2019>, 2019.
- 895 R Core Team. (2013). R: A language and environment for statistical computing. [Available at
896 <http://www.r-project.org/>]
- 897 Raymond, P. A., Hartmann, J., Lauerwald, R., Sobek, S., McDonald, C., Hoover, M., . . .
898 Guth, P. (2013). Global carbon dioxide emissions from inland waters. *Nature*, 503(7476),
899 355–359. Retrieved from <https://doi.org/10.1038/nature12760>
- 900 Regnier, P., Friedlingstein, P., Ciais, P., Mackenzie, F. T., Gruber, N., Janssens, I. A., . . .
901 Thullner, M. (2013). Anthropogenic perturbation of the carbon fluxes from land to ocean.
902 *Nature Geosci.*, 6(8), 597–607. Retrieved from <http://dx.doi.org/10.1038/ngeo1830>
- 903 Ren, W., H. Tian, W.-J. Cai, S. E. Lohrenz, C. S. Hopkinson, W.-J. Huang, J. Yang, B. Tao,
904 S. Pan, and R. He (2016), Century long increasing trend and variability of dissolved organic
905 carbon export from the Mississippi River basin driven by natural and anthropogenic forcing,
906 *Global Biogeochem. Cycles*, 30, 1288–1299, doi:10.1002/2016GB005395.
- 907 Reynolds, C., Jackson, T. & Rawls, W. Estimating available water content by linking 424 the
908 FAO soil map of the world with global soil profile databases and pedo-transfer 425 functions.
909 *Am. Geophys. Union Fall Meet. EOS Trans. Spring Meet. Suppl.* 80, S132 426 (1999).
- 910 Schimel D, Stephens BB, Fisher JB. 2015.Effect of increasing CO2 on the terrestrial carbon
911 cycle. *Proceedings of the National Academy of Sciences, USA* 112: 436–441
- 912 Sheffield, J., Goteti, G., & Wood, E. F. (2006). Development of a 50-Year High-Resolution
913 Global Dataset of Meteorological Forcings for Land Surface Modeling. *Journal of Climate*,
914 19(13), 3088–3111. <https://doi.org/10.1175/JCLI3790.1>
- 915 Silva, T.S.F., Costa, M.P.F. & Melack, J.M. Annual net primary production of macrophytes
916 in the eastern Amazon floodplain. *Wetlands* (2009) 29: 747. <https://doi.org/10.1672/08-107.1>
- 917 Smith, W.K., Fox, A.M., MacBean, N., Moore, D.J.P. and Parazoo, N.C. (2020),
918 Constraining estimates of terrestrial carbon uptake: new opportunities using long-term
919 satellite observations and data assimilation. *New Phytol*, 225: 105-112.
920 doi:[10.1111/nph.16055](https://doi.org/10.1111/nph.16055)
- 921 Spencer, R. G. M., P. J. Hernes, B. Dinga, J. N. Wabakanghanzi, T. W. Drake, and J. Six
922 (2016), Origins, seasonality, and fluxes of organic matter in the Congo River, *Global*
923 *Biogeochem. Cycles*, 30, 1105–1121, doi: 10.1002/2016GB005427.



- 924 Sullivan, M. J. P., Talbot, J., Lewis, S. L., Phillips, O. L., Qie, L., Begne, S. K., ... Zemagho,
925 L. (2017). Diversity and carbon storage across the tropical forest biome. *Scientific Reports*, 7,
926 39102. Retrieved from <https://doi.org/10.1038/srep39102>
- 927 Tathy, J. P., B. Cros, R. A. Delmas, A. Marengo, J. Servant, and M. Labat (1992), Methane
928 emission from flooded forest in central Africa, *J. Geophys. Res.*, 97(D6), 6159–6168,
929 doi:[10.1029/90JD02555](https://doi.org/10.1029/90JD02555).
- 930 Tian, H., Q. Yang, R. G. Najjar, W. Ren, M. A. M. Friedrichs, C. S. Hopkinson, and S. Pan
931 (2015), Anthropogenic and climatic influences on carbon fluxes from eastern North America
932 to the Atlantic Ocean: A process-based modeling study, *J. Geophys. Res. Biogeosci.*, 120,
933 752–772, doi:10.1002/2014JG002760.
- 934 Tyukavina, A., Hansen, M. C., Potapov, P., Parker, D., Okpa, C., Stehman, S. V., ...
935 Turubanova, S. (2018). Congo Basin forest loss dominated by increasing smallholder
936 clearing. *Science Advances*, 4(11). <https://doi.org/10.1126/sciadv.aat2993>
- 937 Valentini, R., Arneth, A., Bombelli, A., Castaldi, S., Cazzolla Gatti, R., Chevallier, F., Ciais,
938 P., Grieco, E., Hartmann, J., Henry, M., Houghton, R. A., Jung, M., Kutsch, W. L., Malhi, Y.,
939 Mayorga, E., Merbold, L., Murray-Tortarolo, G., Papale, D., Peylin, P., Poulter, B.,
940 Raymond, P. A., Santini, M., Sitch, S., Vaglio Laurin, G., van der Werf, G. R., Williams, C.
941 A., and Scholes, R. J.: A full greenhouse gases budget of Africa: synthesis, uncertainties, and
942 vulnerabilities, *Biogeosciences*, 11, 381–407, doi:10.5194/bg11-381-2014, 2014
- 943 Verhegghen, A., Mayaux, P., de Wasseige, C., & Defourny, P. (2012). Mapping Congo Basin
944 vegetation types from 300 m and 1 km multi-sensor time series for carbon stocks and forest
945 areas estimation. *Biogeosciences*, 9(12), 5061–5079. <https://doi.org/10.5194/bg-9-5061-2012>
- 946 Viovy, N. (2018). *CRUNCEP Version 7 - Atmospheric Forcing Data for the Community*
947 *Land Model*. Research Data Archive at the National Center for Atmospheric Research,
948 Computational and Information Systems Laboratory. <http://rda.ucar.edu/datasets/ds314.3/>
- 949 Weiss, L. C., Pötter, L., Steiger, A., Kruppert, S., Frost, U., & Tollrian, R. (2018). Rising
950 pCO₂ in Freshwater Ecosystems Has the Potential to Negatively Affect Predator-Induced
951 Defenses in *Daphnia*. *Current Biology*, 28(2), 327–332.e3.
952 <https://doi.org/https://doi.org/10.1016/j.cub.2017.12.022>
- 953 Williams, C. A., Hanan, N. P., Neff, J. C., Scholes, R. J., Berry, J. A., Denning, A. S., and
954 Baker, D. A.: Africa and the global carbon cycle, *Carbon Balance and Management*, 2(3),
955 doi:10.1186/1750-0680-2-3, 2007.
- 956 Yin, S., Li, X., & Wu, W. (2017). Comparative analysis of NPP changes in global tropical
957 forests from 2001 to 2013. *IOP Conference Series: Earth and Environmental Science*, 57(1),
958 12009. Retrieved from <http://stacks.iop.org/1755-1315/57/i=1/a=012009>
- 959 Zhou, L., Tian, Y., Myneni, R. B., Ciais, P., Saatchi, S., Liu, Y. Y., ... Hwang, T. (2014).
960 Widespread decline of Congo rainforest greenness in the past decade. *Nature*, 509(7498), 86–
961 90. <https://doi.org/10.1038/nature13265>
- 962 Zhuravleva, I., Turubanova, S., Potapov, P., Hansen, M., Tyukavina, A., Minnemeyer, S., ...
963 Thies, C. (2013). Satellite-based primary forest degradation assessment in the Democratic



964 Republic of the Congo, 2000-2010. *Environmental Research Letters*, 8(2), 24034.
965 <https://doi.org/10.1088/1748-9326/8/2/024034>

966

967

968

969



970 *Appendix A*

971

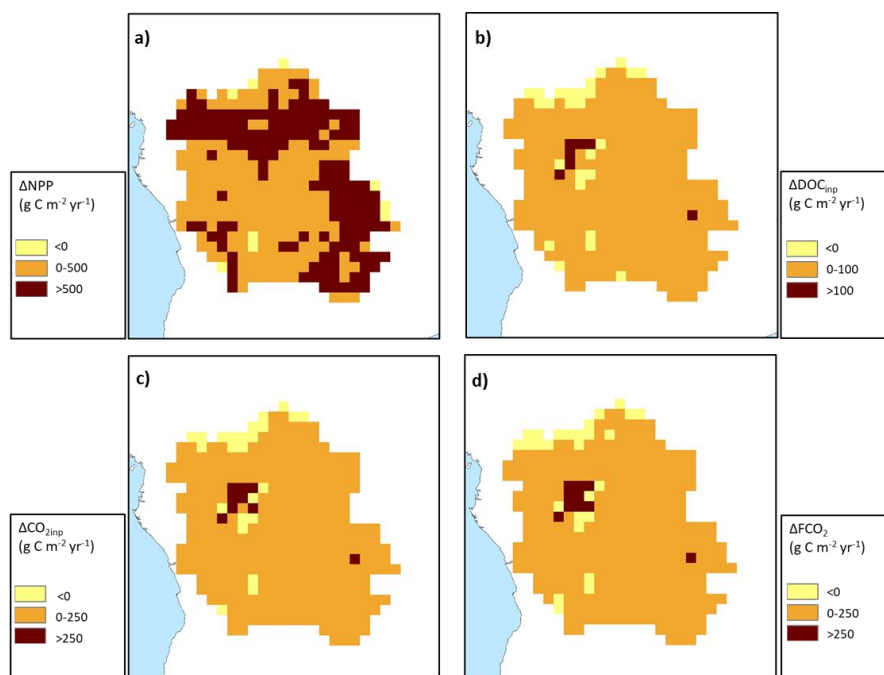
Table A 1: Performance statistics for modelled versus observed seasonality of discharge on the Congo at Brazzaville

Climate forcing	RSME	NSE	R ²	Mean monthly discharge (m ³ s ⁻¹)
ISIMIP	29%	0.20	0.23	38,944
Princeton GPCC	40%	-0.25	0.20	49,784
GSWP3	46%	-4.13	0.04	24,880
CRUNCEP	65%	-15.94	0.01	16,394
Observed (HYBAM)				40,080

972

Table A 2: Pearson correlation coefficient (r) between detrended carbon fluxes and detrended climate variables

	SHR	Aquatic CO ₂ evasion	Lateral C	NEP	Rain	Temp.	MEI
NPP	-0.48	0.68	0.72	0.90	0.64	-0.57	-0.09
SHR		-0.41	-0.48	-0.71	-0.32	0.76	0.04
Aquatic CO ₂ evasion			0.92	0.41	0.87	-0.30	-0.21
Lateral C				0.52	0.81	-0.38	-0.15
NEP					0.40	-0.74	-0.01
Rain						-0.31	-0.26
Temp.							0.03



973

Figure A 1: Change (Δ , 2099 minus 1861) in the spatial distribution of a) terrestrial NPP, b) DOC leaching into the aquatic system, c) CO_2 leaching into the aquatic system and d) aquatic CO_2 evasion. All at a resolution of 1°

974

975

976

977

978

979

980

981

982

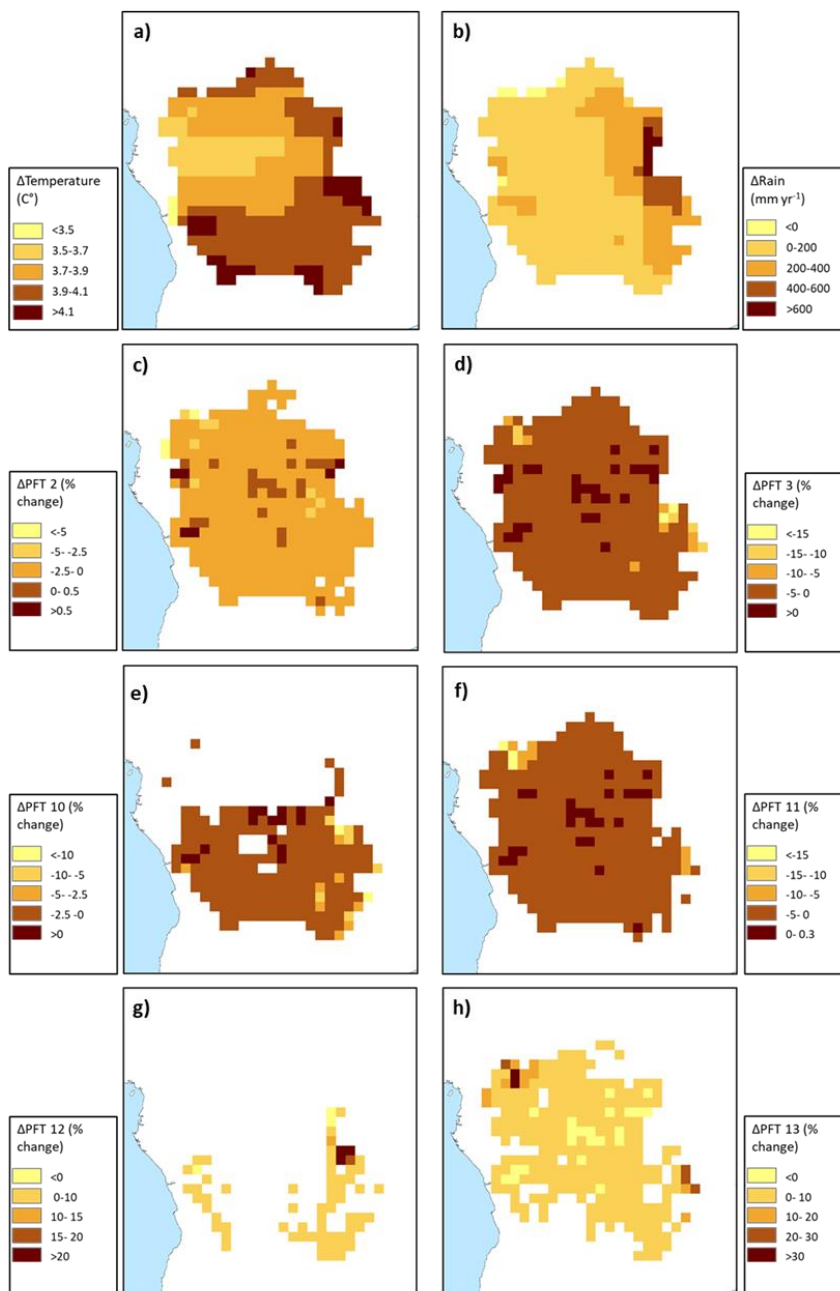


Figure A 2: Change (Δ , 2099 minus 1861) in the spatial distribution of the principal climate and land-use drivers across the Congo Basin; a) mean annual temperature in $^{\circ}\text{C}$, b) mean annual rainfall in mm yr^{-1} , c)-h) mean annual maximum vegetated fraction for PFTs 2,3,10,11,12 and 13. All at a resolution of 1° .



984

985

Period	Temp.	Rain.	PFT2	PFT3	PFT10	PFT11	PFT12	PFT13
1861- 1890	24.0	1451	0.263	0.375	0.154	0.254	0.015	0.014
1981- 2010	25.2	1526	0.255	0.359	0.154	0.255	0.038	0.030
2070- 2099	28.2	1654	0.258	0.362	0.147	0.245	0.039	0.037

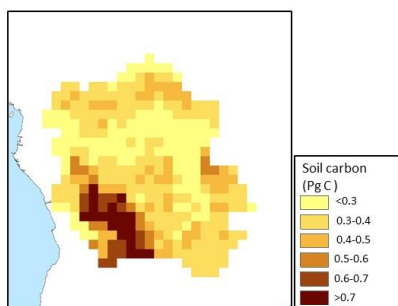


Figure A 3: Spatial distribution of simulated total carbon stored in soils for the present day (1981-2020).

986

987

988